

---

# Perks and Pitfalls of Faithfulness in Regular, Self-Explainable and Domain Invariant GNNs

---

**Steve Azzolin**  
DISI  
University of Trento  
steve.azzolin@unitn.it

**Antonio Longa**  
DISI  
University of Trento  
antonio.longa@unitn.it

**Stefano Teso**  
DISI & CIMEC  
University of Trento  
stefano.teso@unitn.it

**Andrea Passerini**  
DISI  
University of Trento  
andrea.passerini@unitn.it

## Abstract

As Graph Neural Networks (GNNs) become more pervasive, it becomes paramount to build robust tools for computing explanations of their predictions. A key desideratum is that these explanations are *faithful*, *i.e.*, that they portray an accurate picture of the GNN’s reasoning process. A number of different faithfulness metrics exist, begging the question of what is faithfulness exactly, and what are its properties. We begin by showing that existing metrics are not interchangeable – *i.e.*, explanations attaining high faithfulness according to one metric may be unfaithful according to others – and can be systematically insensitive to important properties of the explanation, and suggest how to address these issues. We proceed to show that, surprisingly, optimizing for faithfulness is not always a sensible design goal. Specifically, we show that for injective regular GNN architectures, perfectly faithful explanations are completely uninformative. The situation is different for modular GNNs, such as self-explainable and domain-invariant architectures, where optimizing faithfulness does not compromise informativeness, and is also unexpectedly tied to out-of-distribution generalization.

## 1 Introduction

The increasing popularity of GNNs [1–3] for even high-stakes [4] tasks has prompted the development of tools for explaining their decisions. Regular GNNs are opaque and explanations must be extracted in a post-hoc fashion using specialized algorithms [5], while self-explainable GNNs employ a modular setup to natively output explanations for their own predictions [6]. A key metric of explanation quality is *faithfulness* [4, 7–13]. Intuitively, an explanation is faithful insofar as it highlights all and only those elements – edges and/or node features – of the input graph that are *truly* relevant for the prediction. Faithfulness ensures an explanation portrays an accurate picture of the GNN’s reasoning process, and thus supports understanding, trust modulation, and debugging [14].

Existing faithfulness metrics measure the stability of the model’s output to *perturbations* of the input graph – *e.g.*, to ensure that modifying those elements that are marked as irrelevant by the explanation has in fact no effect – yet differ in many details. For instance, some metrics perturb the input by zeroing-out all irrelevant node features [4] while others delete a subset of edges instead [12]; cf. [Section 3](#) for an overview. Unfortunately, the literature provide little guidance on what metric should be used and on how to tune GNN architectures for optimal faithfulness. We aim to fill this gap.

**Existing metrics are not interchangeable.** As a first contribution, in [Section 3.1](#) we parameterize existing metrics along two dimensions: how *stability* is measured and what *perturbations* are allowed. We show that different parameter choices yield rather different metrics, in the sense that explanations that are faithful for one metric are not faithful according to others. Hence, faithfulness measurements *cannot be interpreted* unless these parameters are provided. This is relevant in high-stakes applications such as loan approval, in which explanation providers could manipulate (but withhold) the parameters to mislead explanation consumers into overestimating the faithfulness of explanations [15].

**Not all existing metrics are equally reliable.** Next, in [Section 3.2](#) we uncover systematic issues with popular faithfulness metrics. Specifically, we show they are *insensitive* to the number of irrelevant elements captured by the explanation, and argue that this issue can be avoided with an appropriate choice of parameters.

**Is faithfulness worth optimizing for?** In [Section 4](#) we study to what extent optimizing for faithfulness is a sensible design goal. We show that for injective GNNs, explanations achieving strict (that is, perfect) faithfulness are not informative, and identify a natural trade-off between expressiveness of the model and usefulness of faithful explanations. Then we show that for modular GNNs, including self-explainable GNNs and GNNs designed for domain invariance, strict faithfulness explanations are not necessarily trivial and evaluate several practical strategies for improving faithfulness, highlighting a trade-off between strict faithfulness and learnability. Finally, in [Section 5](#) we show that faithfulness plays a central, yet so far neglected, role in domain invariance. Specifically, while prior work [16–19] focuses on developing techniques for encouraging GNNs to isolate and use the domain invariant portion of the input, we show that this provides no guarantees unless this subgraph is also faithful.

## 2 Graph Neural Networks and Faithfulness

Throughout, we indicate graphs as  $G = (V, E)$  and annotated graphs as  $G_A = (G, X)$ , where  $\mathbf{x}_u \in \mathbb{R}^d$  are per-node features. We denote the  $k$ -hop neighborhood of  $u$  as  $N_k(u)$ , and shorten  $N_1(u)$  to  $N(u)$ ,  $|G| = |V|$  to  $n$ , and  $\|G\| = |E|$  to  $m$ .

**Graph Neural Networks (GNN)** [1] are discriminative classifiers that, given an input graph  $G_A$ , define a conditional distribution  $p_\theta(\cdot | G_A)$  over candidate labels. In graph classification, the label  $y \in \{1, \dots, c\}$  applies to the whole graph, while in node classification it is a vector  $\mathbf{y} \in \{1, \dots, c\}^n$  with one element per node. Inference in GNNs is *opaque*, in that it relies on message passing of embedding vectors along the graph’s topology. Usually, this amounts to recursively applying an aggregation operation of the form:

$$\mathbf{h}_u^\ell = \text{aggr}(\mathbf{h}_u^{\ell-1}, \{\mathbf{h}_v^{\ell-1} : v \in N(u)\}) \quad (1)$$

to all nodes  $u$ , from the bottom to the top layer. Here,  $\mathbf{h}_u^0 = \mathbf{x}_u$  are the node features,  $\mathbf{h}_u^\ell$  the node embeddings at the  $\ell$ -th layer, and  $\text{aggr}$  a learnable non-linear aggregation function. We refer to this form of aggregation as *local*, as opposed to *non-local* aggregation where  $\text{aggr}$  runs over nodes outside of  $N(u)$ , e.g., by means of virtual nodes [20]. In node classification, the top-layer node embeddings are stacked into a matrix  $H^L \in \mathbb{R}^{n \times d}$ , which is fed to a dense layer to obtain a label distribution  $p_\theta(\mathbf{Y} | G_A) = \text{softmax}(H^L W)$ , where  $W \in \mathbb{R}^{d \times c}$  are weights. In graph classification, they are aggregated into an overall embedding  $\mathbf{h}_G = \text{aggr}_G(\{\mathbf{h}_u^L : u \in V\})$ , also fed to a dense layer.

**Explanations and Faithfulness.** There exist a number of post-hoc techniques [5, 4, 6] that given a GNN  $p_\theta$  can extract a *local explanation* for any target decision  $(G_A, \hat{y})$ . These explanations identify a subgraph  $R_A$  capturing those elements – edges and/or features – deemed relevant for said decision. Unfortunately, explanations output by post-hoc approaches may fail to identify all and only the truly relevant elements, in which case we say they are not *faithful* to the GNN’s reasoning process [5, 4]. Lack of faithfulness hinders understanding, trust allocation, and debugging [14].

This has prompted the development of *self-explainable GNNs* (SE-GNNs), a class of GNNs that natively output explanations without any post-hoc analysis [6, 21]. SE-GNNs comprise two modules: the *detector*  $f$  extracts a class-discriminative subgraph  $R_A$  from the input, and the *classifier*  $g$  uses  $R_A$ , and only  $R_A$ , to infer a prediction. In this context,  $R_A$  acts as a local explanation. Both modules are GNNs, and the detector is encouraged to output human interpretable explanations by leveraging attention [22–25], high-level concepts or prototypes [26–30], or other techniques [31–33].

Metric	Estimates	Divergence $d$	Distribution $q$
Unf [4]	Suf	$\text{KL}(p_\theta(\cdot   G_A), p_\theta(\cdot   G'_A))$	zero out all irrelevant features
Fid- [7–9]		$ p_\theta(\hat{y}   G_A) - p_\theta(\hat{y}   G'_A) $	zero out all irrelevant features, delete all irrelevant edges
RFid- [10–12]		"	delete a random subset of irrelevant edges
PS [13]		$\mathbb{1}\{p_\theta(\hat{y}   G_A) = p_\theta(\hat{y}   G'_A)\}$	multiply all irrelevant elements by relevance scores
Fid+ [7–9]	Nec	$ p_\theta(\hat{y}   G_A) - p_\theta(\hat{y}   G'_A) $	zero out all relevant features, delete all relevant edges
RFid+ [10–12]		"	delete a random subset of relevant edges
PN [13]		$\mathbb{1}\{p_\theta(\hat{y}   G_A) \neq p_\theta(\hat{y}   G'_A)\}$	multiply all relevant elements by relevance scores

Table 1: **Definition 1 recovers existing faithfulness metrics** for appropriate choices of divergence  $d$  and interventional distributions  $p_R$  and  $p_C$ .

In practice, the detector outputs per-element relevance scores (usually in  $[0, 1]$ ), which are then used to identify an explanation subgraph  $R_A$  via, *e.g.*, thresholding. Moreover, the node features  $X^R \in \mathbb{R}^{n \times n}$  of  $R_A$  are derived from, but not necessarily identical to, those of  $G_A$ . These remarks will become relevant when discussing strategies for improving faithfulness in Section 4.2.

**Faithfulness and Domain Invariance.** As we will show in Section 5, faithfulness also plays a key role for *domain-invariant GNNs* (DI-GNNs), which aim to generalize across multiple related domains [16–19]. The underlying assumption is that the label  $y$  and the input  $G_A$  are determined by a set of *domain-invariant* factors. The input graph, however, also contains domain-dependent elements, hence, in order to generalize, the model has to successfully identify and use the invariant subgraph [19, 34]. Like SE-GNNs, DI-GNNs are modular, *i.e.*, include a detector  $f$  for identifying the invariant subgraph  $R_A$  and a classifier  $g$  taking  $R_A$  as input. The detector is encouraged to output invariant subgraphs through specialized regularization terms and training strategies [17, 18, 35, 36].

### 3 Pitfalls of Faithfulness Estimation

In the remainder, we fix a GNN  $p_\theta$  and a decision  $(G_A, \hat{y})$  and study the faithfulness of a corresponding local explanation  $R_A$ . Intuitively, an explanation is faithful as long as it *sufficient*, *i.e.*, if keeping it fixed shields the model’s output from changes to its complement  $C_A$ , and *necessary*, *i.e.*, if altering it affects the model’s output even if the complement  $C_A$  is kept fixed [37–40].

Formally, we say that an explanation  $R_A$  is *strictly sufficient* if no change to the complement  $C_A$  induces any change to the model’s output, *i.e.*,  $\neg \exists C'_A . p_\theta(\cdot | G'_A) \neq p_\theta(\cdot | G_A)$ , where  $G'_A$  is obtained by joining  $R_A$  and  $C'_A$ ; and *strictly necessary* if all changes to the explanation lead to a change, *i.e.*,  $\forall R'_A . p_\theta(\cdot | G'_A) \neq p_\theta(\cdot | G_A)$ , where  $G'_A$  conjoins  $R'_A$  and  $C_A$ . A *strictly faithful* explanation satisfies both conditions. Existing metrics relaxing these notions by restricting the set of alternative graphs  $G'_A$  they consider and by replacing logical equivalence with the expected change in model output [41]. Specifically, *unfaithfulness* [4] estimates sufficiency as the Kullback-Leibler divergence between the original label distribution and that obtained after zeroing-out all irrelevant features from  $G_A$ . *Fidelity minus* [7–9] instead erases all edges and features deemed irrelevant by the explanation and measures the change in likelihood of the prediction  $\hat{y}$ .<sup>1</sup> *Robust fidelity minus* RFid-( $R_A, y$ ) does the same but repeatedly deletes random edges from  $C_A$  [10–12]. Finally, *probability of sufficiency* PS( $R_A, y$ ) estimates how often the model’s prediction changes after multiplying the node features with the relevance scores output by the detector [13]. Metrics for necessity are specular, *i.e.*, they manipulate the input by removing *relevant* elements instead, and include *fidelity plus* Fid+, *robust fidelity plus* RFid+, and *probability of necessity* PN.<sup>2</sup>

While existing metrics differ in many several details, they nicely fit the same common format:

**Definition 1.** Let  $d$  be a divergence,  $p_R$  a distribution over supergraphs of  $R_A$ , and  $p_C$  a distribution over supergraphs of  $C_A$ . Also, let  $\Delta_d(G_A, G'_A) = d(p_\theta(\cdot | G_A) \| p_\theta(\cdot | G'_A))$  measure the impact of replacing  $G_A$  with  $G'_A$  on the label distribution.<sup>3</sup> Then, the **degree of sufficiency** and **degree of necessity** of an explanation  $R_A$  for a decision  $(G_A, \hat{y})$  are:

$$\text{Suf}_{d, p_R}(R_A) = \mathbb{E}_{G'_A \sim p_R}[\Delta_d(G_A, G'_A)], \quad \text{Nec}_{d, p_C}(R_A) = \mathbb{E}_{G'_A \sim p_C}[\Delta_d(G_A, G'_A)] \quad (2)$$

<sup>1</sup>A variant based on the difference in accuracy also exists [8].

<sup>2</sup>In node classification, deleting the explanation never not removes the target node.

<sup>3</sup>We drop the dependency on  $\hat{y}$  for brevity.

The expectations in Eq. (2) are potentially unbounded, but they can be *normalized* to the range  $[0, 1]$ , the higher the better, via a non-linear transformation, *i.e.*, taking  $\exp(-\text{Suf}_{d,p_R}(R_A))$  and  $1 - \exp(-\text{Nec}_{d,p_C}(R_A))$ . Table 1 shows that Definition 1 recovers all existing metrics for appropriate choices of divergence  $d$  and interventional distributions  $p_R$  and  $p_C$ . Alternative choices immediately yield additional metrics.

Both sufficiency and necessity matter, yet there exists a natural tension between them. For instance, explanations covering a larger portion of  $G_A$  likely attain higher sufficiency but lower necessity. This motivates us to define the **degree of faithfulness**  $\text{Faith}_{d,p_R,p_C}(R_A)$  as the harmonic mean of normalized sufficiency and necessity, which is biased towards the lower of the two. We henceforth suppress the dependency on  $d, p_R$  and  $p_C$  whenever it is clear from context.

### 3.1 Faithfulness metrics are not interchangeable

A first key observation is that, despite falling into a common template, existing metrics are *not interchangeable*, in the sense that explanations that are highly faithful according to one metric can be arbitrarily unfaithful for the others. We formalize this in the following proposition:

**Proposition 1.** (Informal.) *Let  $(p_R, p_C)$  and  $(p'_R, p'_C)$  two pairs of interventional distributions. Then, depending on  $p_\theta$  and  $G_A$ ,  $|\text{Suf}_{d,p_R}(R_A) - \text{Suf}_{d,p'_R}(R_A)|$  and  $|\text{Nec}_{d,p_C}(R_A) - \text{Nec}_{d,p'_C}(R_A)|$  can be as large as the natural range of  $d$ .*

All proofs (as well as relevant discussion) can be found in Appendix A. In essence, Proposition 1 means that faithfulness results cannot be properly interpreted unless the parameters  $d, p_R$  and  $p_C$  are known. In practice, this entails that explanation producers – such as banks and algorithm designers – responsible for certifying the faithfulness of explanations cannot withhold the parameters used in the computation, least end-users blindly trust explanations that are not sufficiently faithful for their down-stream applications.

### 3.2 Not all faithfulness estimators are equally good

Given this large variety of metrics, it is natural to wonder whether they are all equally good. As we will show, it turns out this is not the case because – surprisingly – commonly used necessity metrics are *insensitive* to the number of irrelevant edges in the explanation.

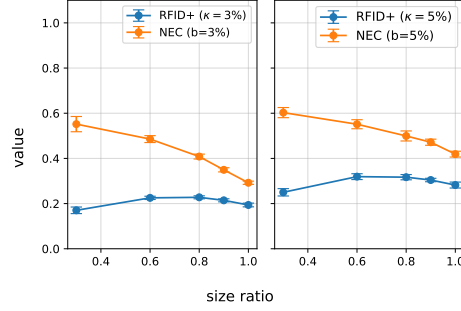
**Fid+ is systematically invariant to truly irrelevant edges.** In the following, we assume  $R_A$  contains  $m$  truly relevant edges, that is, such that if any of them is removed from  $G$  yield a new graph  $G'$  such that  $\Delta(G, G') \neq 0$ . We begin by showing that metrics that estimate necessity using a single modified graph  $G'_A$  obtained by deleting the whole explanation  $R_A$ ,<sup>4</sup> such as Fid+, suffer from this issue. To see this, note that in an  $L$ -layer GNN with local aggr, messages from nodes outside of  $N_L(u)$  cannot influence the prediction of node  $u$ . Now, consider a 1-layer GNN  $p_\theta$  for node classification and an input line graph  $u_1 \leftarrow u_2 \leftarrow \dots \leftarrow u_n$ . Since there is only one layer, only the messages from  $N_1(u_1) = \{u_1, u_2\}$  can contribute to the distribution of  $Y_1$ . However, Fid+ associates the same value to both  $R_A = N_2(u_1)$  and to  $R'_A = G_A$ , which contains arbitrarily many irrelevant nodes. In fact, for  $R_A$  it deletes  $u_2$ , while for  $R'_A$  it deletes  $u_2, \dots, u_n$ : in both cases, the model predicts  $Y_1$  using  $x_1$  only, meaning that Fid+ will attain the same value. Note that, when the edge relevance scores are binary, PN behaves exactly like Fid+, in which case it also suffers from this issue.

**RFid+ is systematically invariant to truly irrelevant edges.** So does RFid+. To see this, consider a 1-layer GNN for node prediction, and let  $G_A$  be an  $n$ -node star graph with  $u_1$  as its center, and assume that only the edges between  $u_1, u_2$  and  $u_3$  are truly relevant to  $p_\theta(Y_1 | G_A)$ . Now, take two explanations:  $R = \{u_1, u_2, u_3\}$  covers all and only the truly relevant edges, and  $R' = G$ . Like above, it turns out that  $\text{RFid+}(R) = \text{RFid+}(R')$ . In fact, RFid+ estimates necessity by removing edges in an IID fashion, which means that the probability that it deletes the edges between  $u_1, u_2$ , and  $u_3$  from  $R$  is the same regardless of how many other edges appear in the explanation. We formalize this intuition in the following result:

**Proposition 2.** *Fix a divergence  $d$  and a threshold  $\epsilon > 0$ . Let  $R$  contain  $r$  truly relevant edges. Then,  $\text{RFid+}(R)$  does not depend on  $\|R\| - r$ .*

<sup>4</sup>In node classification, the node whose prediction is being explained is not removed even if it belongs to  $R$ .

Figure 1: **Dependency of the necessity metrics on the size of the explanation.** RFid+ and Nec of explanations output by LECI on Motif2-Basis (averaged over 5 seeds) for different explanation sizes (x-axis) and metric hyper-parameter  $\kappa, b \in \{3\%, 5\%\}$ . RFid+ assigns similar or even higher scores to larger explanations, while Nec (with a budget  $b$  proportional to the average graph size  $\bar{m}$ ) decreases for increasing explanation size, as expected.



The question is then how to instantiate Nec such that it *does* depend on the number of irrelevant elements. We next show that this can be achieved by letting  $p_C$  be the *uniform distribution* over all subgraphs of  $R_A$ . Since marginalizing over all subgraphs is intractable, we also show that simply averaging over a smaller subset of graphs obtained by erasing  $b$  edges from the explanation itself also avoids the issue. We summarize our findings as follows:

**Proposition 3.** Fix any divergence  $d$  and a constant budget  $b \geq 1$ . Let  $\mathcal{S}_R^b$  be the set of subgraphs of  $G$  obtained by deleting  $b$  edges from  $R$  while keeping  $C$  fixed, and  $\mathcal{A}_R^b = \{G' \in \mathcal{S}_R^b : \Delta(G, G') \geq \epsilon\}$  those subgraphs that lead to a large enough change in  $\Delta$ . Also, let  $\mathcal{S}_R = \mathcal{S}_R^1 \cup \dots \cup \mathcal{S}_R^m$  and similarly for  $\mathcal{A}_R$ . Given an explanation  $R$  containing  $r$  truly relevant edges,  $\text{Nec}(R)$  computed using a uniform  $p_C$  over  $\mathcal{S}_R$  depends on the number of irrelevant edges  $\|R\| - r$ . The same holds if  $\text{Nec}(R)$  is computed using a uniform  $p_C$  over  $\mathcal{S}_R^b$ .

This result highlights that, by selecting an appropriate interventional distribution  $p_C$ , it is possible to design a necessity metric that appropriately accounts for the number of irrelevant edges.

**The choice of budget  $b$  can bias necessity.** In fact, Proposition 3 may fail if  $b$  depends on the size of the input graph or the size of the explanation. This occurs because the numerator and denominator of  $|\mathcal{A}_R^b|/|\mathcal{S}_R^b|$  both depend on  $b$ , and thus can act as a confounding variable. Specifically, if  $b$  depends on  $\|R\|$ , the metric – once again – does not properly account for irrelevant items in the explanation, as the number of deletions increases according to the size of the explanation. Indeed, a numerical simulation shows that the probability of deleting at least one truly relevant edge does not depend on the number of irrelevant ones in the explanation, if  $b$  is proportional to the explanation size (see Fig. 4 in the Appendix). On the other hand, if  $b$  is proportional to the size of the input graph  $G$ , the number of deletions depends also on the size of the complement, resulting in a metric confounded by the complement of the explanation.<sup>5</sup> This is best seen in the following example:

**Example 1.** Fix an explanation  $R$  composed of two edges, only one of which is truly relevant. If  $G$  has 10 edges, fixing a budget of deletion as 10% of the graph size yields a modified graph  $G'$  such that  $P(G' \in \mathcal{A}_R^1) = \frac{1}{2}$ . Instead, if  $G$  has 20 edges, then  $P(G' \in \mathcal{A}_R^2) = 1$ . Hence, despite  $R$  being fixed, the probability of sampling truly relevant edges drastically changes.

We propose to avoid these issues by fixing a budget that is proportional to a data set-wide statistic, such as average graph size  $\bar{m} = 1/|\mathcal{D}| \sum_{G \in \mathcal{D}} \|G\|$ , where  $\mathcal{D}$  is the set of graphs. This way, it no longer directly depends on the size of any specific input graph or explanation, while still being adaptive to the target task.

Based on these observations, in our experiments we adopt a uniform  $p_C(G)$  over subgraphs of size  $\|G\| - b$ , where  $b$  is a hyper-parameter, which will be denoted as  $p_C^b(G)$ . The practical difference between RFid+ and Nec with  $p_C^b$  is exemplified in the following analysis, where we evaluate the necessity of explanations of the modular architecture GSAT [22] over the benchmark Motif2-Basis [43], and for different RFid+ edge-deletion probability  $\kappa$  and budget  $b$ . Since GSAT outputs explanation scores in the  $[0, 1]$  range, we obtain a relevant input subgraph by discretizing the explanation mask at different size ratios, as common in XAI evaluation [5, 9]. The results provided in Fig. 1 show that RFid+ assigns close-to-constants scores to explanations at different size ratios, while

<sup>5</sup>From a causal perspective, letting  $b$  depend on the size of  $G$  opens a backdoor path from  $G$  to Nec, confounding Nec [42].



our previously discussed Nec tends to penalize larger explanation. We provide in [Appendix C.2](#) a further comparison of the two metrics.

## 4 Is Faithfulness Worth Optimizing For?

We show that for regular injective GNNs, strict faithful explanations are trivial, highlighting a trade-off between explainability and expressivity. For modular GNNs, instead, non-trivial strictly faithful explanations are possible provided certain conditions are met. We then empirically verify that some of these conditions are hard to achieve for practical models, suggesting a trade-off between strict faithfulness and learnability.

### 4.1 The Case of Regular GNNs

Recall that an explanation is strictly faithful (cf. [Section 3](#)) when no change to the complement  $C_A$  of  $R_A$  affects the model’s output, and when all elements in  $R_A$  contribute to the final prediction. In the following, we show that for regular GNNs strictly faithful explanations are *completely uninformative*. To build intuition, notice that strictly sufficient explanations must subsume the computational graph of the prediction, that is, the subgraph of  $G_A$  induced by all nodes whose messages influence the label distribution. In node classification, this is the  $L$ -hop neighborhood of the target node, and in graph classification the whole input graph. More formally:

**Proposition 4.** *Consider a binary classification task and an  $L$ -layer injective GNN: i) For **node classification** that only uses local aggregators. Then an explanation  $R_A$  for a decision  $(G_A, \hat{y}_u)$  is strictly faithful wrt  $p_R$  iff it subsumes  $N_L(u)$ . ii) For **graph classification**. Then an explanation  $R_A$  for a decision  $(G_A, \hat{y})$  is strictly faithful wrt  $p_R$  iff it subsumes all of  $G_A$ .*

Note that in both cases the explanation does not depend on the learned weights at all, hence strictly faithful explanations are *trivial*. This is a direct consequence of injectivity, a prerequisite for GNNs to implement the Weisfeiler-Lehman test [44, 45], and highlights a trade-off between expressivity and explainability.<sup>6</sup> For regular GNNs, even forgoing injectivity does not give an easy way to obtain non-trivial strictly faithful explanations. In the next section, we show how this is instead attainable with modular GNN architectures.

### 4.2 The Case of Modular GNNs

For modular GNNs like SE-GNNs and DI-GNNs, non-trivial strictly faithful explanations are attainable, at least in theory. In fact, the following proposition characterizes a set of simple architectural choices making strict faithfulness achievable:

**Proposition 5.** *Consider a binary classification task. Let  $p_\theta$  be a modular GNN with detector  $f$  and an injective classifier  $g$  for graph or node classification. If  $f$  is stable, i.e., it always predicts the same  $R_A$  for all  $G'_A \sim p_R$ , and implements all of the following strategies:*

- **Hard Scores (HS):** it outputs binary 0–1 relevance scores;
- **Content Features (CF):** the node features of  $R_A$  are taken directly from the node features of  $G_A$ ;
- **Explanation Readout (ER):** (for graph classification only)  $\text{aggr}_G$  only aggregates embeddings from  $R_A$  (as opposed to all of  $G_A$ );

then  $R_A$  is strictly faithful.

By additionally choosing  $f$  to be non-injective, non-trivial strictly faithful explanations can be obtained. Albeit not strictly necessary if the strategies in [Proposition 5](#) are in place, another useful strategy is ensuring the locality of the aggregation function  $\text{aggr}$  (**LA**), as non-local aggregations (cf. [Section 2](#)) can easily mix the information of the explanation with that of its complement, and can create unwanted dependencies between any pair of nodes in the graph.

<sup>6</sup>Of course, one can obtain more informative explanations by giving up on strict faithfulness and instead aiming at producing explanations that are both faithful enough and smaller than the entire computational graph.

Despite their simplicity, these strategies can greatly impact expressivity and learning in practice. In fact, binary relevance scores (prescribed by **HS**) are notoriously hard to differentiate through [24, 46–48], and non-local aggregators (forbidden by **LA**) are popular choices to increase the expressivity of GNNs [49, 50, 20]. Overall, Table 2 testifies that most popular modular models indeed lack one or more of the above desiderata in favor of better downstream performance.

In the remainder of this section, we empirically investigate the impact of integrating popular modular architectures with the strategies they lack, measuring their effect on both faithfulness and final accuracy.

**Experimental setup:** We benchmarked six representative modular architectures, listed in Table 2, following their respective evaluation testbed for graph classification. The datasets chosen for evaluation are picked from the usual evaluation routines for respectively SE-GNNs and DI-GNNs. For DI-GNNs, the chosen benchmarks can be divided into datasets with known domain-invariant input motifs (Motif2-Basis, CMNIST-Color), datasets with presumed domain-invariant input motifs (LBAPcore), and datasets where domain-invariant input motif are not expected (SST2). This last case is especially problematic, as no clear advantage is expected in focusing on a subset of the input graph. The full experimental setup is detailed in Appendix B.

**Results and discussion:** Table 3 and Table 4 show the results for the base SE-GNNs and DI-GNNs architectures and their augmented variants. The results suggest that it is possible to improve faithfulness by applying the missing strategies above, yet not consistently across strategies, models, and datasets. Specifically, the strategy with the lightest impact on model architecture, namely **ER**, is the one achieving the best results, improving faithfulness over the base model in 13 out of 21 cases and being on par in 4. Conversely, more impactful strategies like **HS** and **LA** yield less consistent results. For example, **HS** severely compromises the training of GSAT in Motif2-Basis and Motif-Size, resulting in a train and test accuracy around 50%. When combining strategies, faithfulness generally improves when the individual strategies yield positive results. Among all datasets, SST2 is confirmed to be the most difficult to improve on. Indeed, models tend to output explanations that cover the entire input graph for this dataset (see Appendix C.1 for the details).

These results suggest that, while potentially useful, strict faithfulness is a hard goal to achieve and not all strategies encouraging it are viable in practice. Increasing the degree of faithfulness is a convenient strategy when strict faithfulness is out of reach. Necessity can intuitively be encouraged via sparsification techniques [23, 51], whereas encouraging stability of the detector  $f$  (using approaches like contrastive learning [35, 17], adversarial training [18], or data augmentation [25]) is a natural option for encouraging sufficiency, *regardless* of the properties of the classifier  $g$  built on top of it.

Finally, results in Table 4 show instances of DI-GNNs where faithfulness-enforcing strategies also improved OOD generalization abilities. In the next section we formally investigate the relationship between faithfulness and OOD generalization.

## 5 The Importance of Faithfulness for Domain Invariance

Finally, we study the impact of faithfulness – and lack thereof – on domain invariance. In the domain invariance literature [18, 35], one distinguishes between in-distribution (ID) and out-of-distribution (OOD) data, sampled from  $p^{id}(G_A, Y)$  and  $p^{ood}(G_A, Y)$ , respectively, and the goal is to learn a DI-GNN  $p_\theta$  that generalizes from ID to OOD data. We begin by showing that, even if the graphs  $R_A$  extracted by a DI-GNN (cf. Section 2) are domain invariant, unless they are also strictly sufficient, the model’s prediction is *not* domain invariant.

**Proposition 6.** *Let  $p_\theta$  be a modular DI-GNN such that the detector  $f$  outputs graphs  $R_A$  that are maximally domain-invariant, i.e., that comprise all and only those elements that are constant across the target domains. If  $R_A$  is not strictly sufficient, then the prediction is not domain invariant.*

Model	HS	ER	CF	LA
GISST [23]	✗	✗	✓	✓
GSAT [22]	✗	✗	✓	✗/✓
RAGE [51]	✗	✗	✓	✓
CIGA [35]	TopK	✓	✗/✓	✗/✓
GSAT [22]	✗	✗	✓	✗/✓
LECI [18]	✗	✗	✓	✗/✓

Table 2: **Popular modular architectures fail to fully implement faithfulness-enforcing strategies.** SE-GNNs at the top and DI-GNNs on the bottom. ✗/✓ means that both variants exist and the choice is made via cross-validation.

Dataset	BaMS		Motif2		Motif-Size		BBBP	
	Acc	Faith	Acc	Faith	Acc	Faith	Acc	Faith
GSAT	100 ± 00	35 ± 03	92 ± 01	61 ± 01	90 ± 01	60 ± 02	79 ± 04	27 ± 08
GSAT + ER	100 ± 00	35 ± 03	92 ± 01	63 ± 01	90 ± 01	65 ± 01	80 ± 02	33 ± 04
GSAT + HS	98 ± 01	21 ± 06	53 ± 02	24 ± 05	54 ± 03	22 ± 05	71 ± 01	31 ± 09
GSAT + ER + HS	99 ± 01	24 ± 04	57 ± 04	37 ± 03	56 ± 07	29 ± 09	73 ± 02	33 ± 02
GISST	100 ± 00	25 ± 03	92 ± 01	53 ± 02	92 ± 00	50 ± 02	84 ± 03	23 ± 11
GISST + ER	-	-	-	-	-	-	85 ± 06	27 ± 06
GISST + HS	-	-	-	-	-	-	83 ± 05	19 ± 07
GISST + ER + HS	-	-	-	-	-	-	81 ± 07	15 ± 09
RAGE	96 ± 01	33 ± 05	83 ± 02	64 ± 04	74 ± 09	63 ± 07	82 ± 01	33 ± 04
RAGE + ER	96 ± 02	33 ± 02	85 ± 06	66 ± 03	71 ± 09	55 ± 07	84 ± 01	33 ± 05
RAGE + HS	97 ± 01	46 ± 03	85 ± 01	65 ± 02	78 ± 07	65 ± 09	84 ± 02	46 ± 02
RAGE + ER + HS	96 ± 01	46 ± 04	83 ± 04	64 ± 04	75 ± 08	62 ± 12	82 ± 01	43 ± 03

Table 3: Test set accuracy and faithfulness of SE-GNNs augmented with the strategies delineated in Proposition 5, averaged over 5 seeds. Improvements over the base model are in green, worsenings in red. We do not augment GISST on BaMS, Motif2-Basis, and Motif-Size since these data sets have constant input features for all nodes, meaning that these strategies have no effect.

Dataset	Motif2		CMNIST		LBAPcore		SST2	
	Acc	Faith	Acc	Faith	Acc	Faith	Acc	Faith
LECI	85 ± 07	58 ± 02	26 ± 10	48 ± 11	71 ± 01	37 ± 03	83 ± 01	26 ± 02
LECI + ER	86 ± 03	59 ± 02	58 ± 12	58 ± 03	71 ± 01	42 ± 04	82 ± 01	13 ± 02
LECI + HS	86 ± 04	57 ± 02	34 ± 10	57 ± 01	72 ± 01	25 ± 02	83 ± 01	18 ± 03
LECI + LA	-	-	46 ± 11	57 ± 03	69 ± 01	36 ± 09	81 ± 05	20 ± 04
LECI + ER + HS + LA	79 ± 11	55 ± 02	75 ± 06	61 ± 01	59 ± 02	24 ± 01	81 ± 02	16 ± 01
CIGA	46 ± 10	38 ± 08	23 ± 03	36 ± 03	69 ± 01	20 ± 10	76 ± 06	18 ± 01
CIGA + ER	45 ± 09	54 ± 04	23 ± 02	43 ± 07	59 ± 07	07 ± 03	74 ± 03	16 ± 01
CIGA + CF	53 ± 07	49 ± 02	13 ± 01	49 ± 09	49 ± 12	04 ± 01	55 ± 07	09 ± 12
CIGA + LA	41 ± 00	39 ± 05	30 ± 09	41 ± 03	68 ± 01	25 ± 17	79 ± 03	16 ± 01
CIGA + ER + CF + LA	47 ± 08	39 ± 07	23 ± 03	50 ± 02	66 ± 01	28 ± 17	76 ± 08	15 ± 02
GSAT	75 ± 06	58 ± 01	25 ± 04	48 ± 03	70 ± 03	32 ± 06	79 ± 04	22 ± 04
GSAT + ER	59 ± 06	60 ± 06	30 ± 06	48 ± 01	67 ± 01	36 ± 03	81 ± 01	23 ± 04
GSAT + HS	86 ± 03	42 ± 07	14 ± 03	44 ± 04	71 ± 01	30 ± 01	80 ± 02	17 ± 02
GSAT + LA	63 ± 08	58 ± 01	27 ± 03	46 ± 04	69 ± 03	39 ± 05	81 ± 01	21 ± 04
GSAT + ER + HS + LA	64 ± 08	47 ± 03	17 ± 02	51 ± 05	70 ± 01	33 ± 04	80 ± 01	17 ± 01

Table 4: OOD test set accuracy and faithfulness of DI-GNNs augmented with the strategies delineated in Proposition 5, averaged over 5 seeds.

This result is significant because DI-GNNs typically optimize only for domain invariance of the extracted subgraph  $R_A$ , neglecting how this is then used by the classifier on top. The next result highlights that the degree of faithfulness of  $R_A$  – and specifically, that of sufficiency – plays a direct role in ensuring the model predictions are in fact domain invariant.

**Theorem 1.** (Informal) Let  $p_\theta$  be a deterministic DI-GNN with detector  $f$  and classifier  $g$ , and  $p^{id}(G_A, Y)$  and  $p^{ood}(G_A, Y)$  be the ID and OOD empirical distributions, respectively. Then:

$$\left| \mathbb{E}_{(G_A, y) \sim p^{id}} [p_\theta(y | G_A)] - \mathbb{E}_{(G_A, y) \sim p^{ood}} [p_\theta(y | G_A)] \right| \leq \mathbb{E}_{R_A^*} \left[ k_1 (\lambda_{topo}^{id} + \lambda_{topo}^{ood}) + k_2 (\lambda_{feat}^{id} + \lambda_{feat}^{ood}) + (\lambda_{suff}^{id} + \lambda_{suff}^{ood}) \right]. \quad (3)$$

Here,  $\mathbb{E}_{R_A^*}$  runs over all possible maximally invariant subgraphs,  $k_1, k_2 > 0$  are Lipschitz constants of  $p_\theta$ ,  $\lambda_{topo}^{id}$ ,  $\lambda_{topo}^{ood}$ ,  $\lambda_{feat}^{id}$ , and  $\lambda_{feat}^{ood}$  measure the (negated) degree of domain invariance of the detector’s output (with respect to topology and features, respectively), and  $\lambda_{suff}^{id}$ ,  $\lambda_{suff}^{ood}$  are the degree of sufficiency for ID and OOD data.

Note that the degree of invariance is computed as the *plausibility* [5] of  $R_A$  with respect to the (domain-invariant) ground truth. In essence, Theorem 1 shows that a DI-GNN has a consistent



behavior between ID and OOD data if i)  $R_A$  is in fact invariant across domains, and ii)  $R_A$  is highly sufficient.

We stress that while necessity does not appear in the bound, it becomes important if we wish the invariant subgraph to be non-trivial and human-understandable. Indeed, Fig. 2 shows a statistically significant anti-correlation (Pearson’s correlation  $-0.83$ ,  $p$ -value 0.01) between the difference in average prediction’s likelihood between ID and OOD data, and the combination of the degree of domain-invariance and faithfulness. Notably, the same applies, yet with a slightly weaker correlation of  $-0.74$  ( $p$ -value 0.02), when replacing likelihood with accuracy. See Appendix B for further details.

## 6 Related Work

**Modular architectures.** Modular GNNs have become a popular architectural design choice for seeking trustworthiness, either in the form of explainable [23, 24, 33, 51] or confounding-free predictions [25, 17, 18, 35] (see Jiang et al. [19] for a detailed survey), also in deep neural networks for non-relational data [52, 53]. In both settings, the quality of the explanation – or any other sparse representation used to communicate across the two modules – is known to play a crucial role, for users and stakeholders, and for ensuring fair and generalizable model outputs [5, 9, 22]. Despite being designed primarily for faithfulness, as the prediction depends on the explanation only, little attention has been paid to measuring *how well* the classifier adheres its own explanations, an issue that can completely prevent trust allocation [54]. Indeed, recent work has shown how for popular SE-GNNs architectures, the classifier seems to be more faithful to randomly generated subgraphs than to its own explanations [21]. In this work, we investigate the reasons for this behavior, discuss the applicability of faithfulness-enforcing strategies and extend the analysis to DI-GNNs.

**Faithfulness.** In the Explainable AI [55] and GNN literature [4], sufficiency and faithfulness are often conflated, however explanations that are not necessary cannot be faithful, as they open to trivially sufficient yet uninformative explanations. Faithfulness is also sometimes defined as the correlation between the explainers “performance” and that of the model, that is, to what extent corrupting the input alters the model’s performance [41]. However, this is narrow to model and explainer performance and does not reflect the degree to which a classifier relies on the provided explanation for making its prediction. Our notion of faithfulness is rooted in notions from causal explainability [38] and disentanglement in causal representation learning [56, 57]. Like Beckers [38], we argue that absolute measurements of sufficiency, and more generally faithfulness, are uninformative unless properly contextualized, in our case by the choice of parameters used for the measurements. Following [15], we argue this leaves room for adversarial explanation providers to supply explanations that optimize their objective rather than that of the explanation consumer.

## 7 Discussion and Broader Impact

We have studied the faithfulness of explanations in regular and modular GNNs. Our results indicate that, despite conforming to a shared template, existing faithfulness metrics are *not* interchangeable and in fact some even suffer from systematic issues, which we show can be avoided with an appropriate choice of hyperparameters. We have also shown that optimizing for faithfulness is not always a sensible design goal, and analyzed – theoretically and empirically – both strategies for improving faithfulness in modular GNNs and the importance of faithfulness for domain invariance. From a societal perspective, the aim of this work is to shed light on the non-trivial nature of explanation faithfulness, warning against its unqualified reporting and interpretation. It can thus contribute to the development of truly interpretable and trustworthy models for networked data.

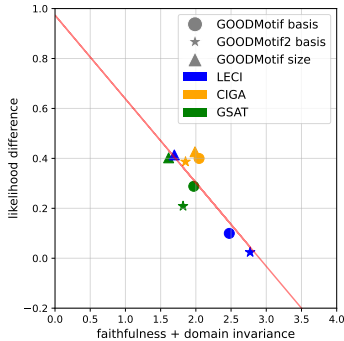


Figure 2: **Likelihood, faithfulness and domain-invariance are correlated.** The plot shows the difference in likelihood between splits. The red line is the best linear fit. Best viewed in color.

## References

- [1] Franco Scarselli, Marco Gori, Ah Chung Tsoi, Markus Hagenbuchner, and Gabriele Monfardini. The graph neural network model. *IEEE transactions on neural networks*, 20(1):61–80, 2008.
- [2] Thomas N Kipf and Max Welling. Semi-supervised classification with graph convolutional networks. *arXiv preprint arXiv:1609.02907*, 2016.
- [3] Petar Veličković, Guillem Cucurull, Arantxa Casanova, Adriana Romero, Pietro Liò, and Yoshua Bengio. Graph attention networks. In *International Conference on Learning Representations*, 2018.
- [4] Chirag Agarwal, Owen Queen, Himabindu Lakkaraju, and Marinka Zitnik. Evaluating explainability for graph neural networks. *Scientific Data*, 10(1):144, 2023.
- [5] Antonio Longa, Steve Azzolin, Gabriele Santin, Giulia Cencetti, Pietro Liò, Bruno Lepri, and Andrea Passerini. Explaining the explainers in graph neural networks: a comparative study. *arXiv preprint arXiv:2210.15304*, 2022.
- [6] Jaykumar Kakkad, Jaspal Jannu, Kartik Sharma, Charu Aggarwal, and Sourav Medya. A survey on explainability of graph neural networks. *arXiv preprint arXiv:2306.01958*, 2023.
- [7] Phillip E Pope, Soheil Kolouri, Mohammad Rostami, Charles E Martin, and Heiko Hoffmann. Explainability methods for graph convolutional neural networks. In *Proceedings of the IEEE/CVF conference on computer vision and pattern recognition*, pages 10772–10781, 2019.
- [8] Hao Yuan, Haiyang Yu, Shurui Gui, and Shuiwang Ji. Explainability in graph neural networks: A taxonomic survey. *IEEE transactions on pattern analysis and machine intelligence*, 45(5): 5782–5799, 2022.
- [9] Kenza Amara, Zhitao Ying, Zitao Zhang, Zhichao Han, Yang Zhao, Yinan Shan, Ulrik Brandes, Sebastian Schemm, and Ce Zhang. Graphframex: Towards systematic evaluation of explainability methods for graph neural networks. In *Learning on Graphs Conference*, pages 44–1. PMLR, 2022.
- [10] Tianxiang Zhao, Dongsheng Luo, Xiang Zhang, and Suhang Wang. Towards faithful and consistent explanations for graph neural networks. In *Proceedings of the Sixteenth ACM International Conference on Web Search and Data Mining, WSDM ’23*, page 634–642, New York, NY, USA, 2023. Association for Computing Machinery. ISBN 9781450394079. doi: 10.1145/3539597.3570421. URL <https://doi.org/10.1145/3539597.3570421>.
- [11] Kenza Amara, Mennatallah El-Assady, and Rex Ying. GInx-eval: Towards in-distribution evaluation of graph neural network explanations. In *XAI in Action: Past, Present, and Future Applications*, 2023. URL <https://openreview.net/forum?id=w6Qnoy2RXG>.
- [12] Xu Zheng, Farhad Shirani, Tianchun Wang, Wei Cheng, Zhuomin Chen, Haifeng Chen, Hua Wei, and Dongsheng Luo. Towards robust fidelity for evaluating explainability of graph neural networks, 2023.
- [13] Juntao Tan, Shijie Geng, Zuohui Fu, Yingqiang Ge, Shuyuan Xu, Yunqi Li, and Yongfeng Zhang. Learning and evaluating graph neural network explanations based on counterfactual and factual reasoning. In *Proceedings of the ACM Web Conference 2022, WWW ’22*, page 1018–1027, New York, NY, USA, 2022. Association for Computing Machinery. ISBN 9781450390965. doi: 10.1145/3485447.3511948. URL <https://doi.org/10.1145/3485447.3511948>.
- [14] Stefano Teso, Öznur Alkan, Wolfgang Stammer, and Elizabeth Daly. Leveraging explanations in interactive machine learning: An overview. *Frontiers in Artificial Intelligence*, 2023.
- [15] Sebastian Bordt, Michèle Finck, Eric Raidl, and Ulrike von Luxburg. Post-hoc explanations fail to achieve their purpose in adversarial contexts. In *Proceedings of the 2022 ACM Conference on Fairness, Accountability, and Transparency*, pages 891–905, 2022.
- [16] Hengrui Cai, Yixin Wang, Michael Jordan, and Rui Song. On learning necessary and sufficient causal graphs, 2023.

- [17] Yongqiang Chen, Yatao Bian, Kaiwen Zhou, Binghui Xie, Bo Han, and James Cheng. Rethinking invariant graph representation learning without environment partitions. 2023.
- [18] Shurui Gui, Meng Liu, Xiner Li, Youzhi Luo, and Shuiwang Ji. Joint learning of label and environment causal independence for graph out-of-distribution generalization. *arXiv preprint arXiv:2306.01103*, 2023.
- [19] Wenzhao Jiang, Hao Liu, and Hui Xiong. Survey on trustworthy graph neural networks: From a causal perspective, 2023.
- [20] Florian Sestak, Lisa Schneckenteiler, Johannes Brandstetter, Sepp Hochreiter, Andreas Mayr, and Günter Klambauer. Vn-egnn: E(3)-equivariant graph neural networks with virtual nodes enhance protein binding site identification, 2024.
- [21] Marc Christiansen, Lea Villadsen, Zhiqiang Zhong, Stefano Teso, and Davide Mottin. How faithful are self-explainable gnns? *arXiv preprint arXiv:2308.15096*, 2023.
- [22] Siqi Miao, Mia Liu, and Pan Li. Interpretable and generalizable graph learning via stochastic attention mechanism. In *International Conference on Machine Learning*, pages 15524–15543. PMLR, 2022.
- [23] Chris Lin, Gerald J Sun, Krishna C Bulusu, Jonathan R Dry, and Marylens Hernandez. Graph neural networks including sparse interpretability. *arXiv preprint arXiv:2007.00119*, 2020.
- [24] Giuseppe Serra and Mathias Niepert. Learning to explain graph neural networks. *arXiv preprint arXiv:2209.14402*, 2022.
- [25] Ying-Xin Wu, Xiang Wang, An Zhang, Xiangnan He, and Tat-Seng Chua. Discovering invariant rationales for graph neural networks. *arXiv preprint arXiv:2201.12872*, 2022.
- [26] Zaixi Zhang, Qi Liu, Hao Wang, Chengqiang Lu, and Cheekong Lee. Protgnn: Towards self-explaining graph neural networks. In *Proceedings of the AAAI Conference on Artificial Intelligence*, volume 36, pages 9127–9135, 2022.
- [27] Alessio Ragno, Biagio La Rosa, and Roberto Capobianco. Prototype-based interpretable graph neural networks. *IEEE Transactions on Artificial Intelligence*, 2022.
- [28] Enyan Dai and Suhang Wang. Towards self-explainable graph neural network. In *Proceedings of the 30th ACM International Conference on Information & Knowledge Management*, pages 302–311, 2021.
- [29] Enyan Dai and Suhang Wang. Towards prototype-based self-explainable graph neural network. *arXiv preprint arXiv:2210.01974*, 2022.
- [30] Lucie Charlotte Magister, Pietro Barbiero, Dmitry Kazhdan, Federico Siciliano, Gabriele Ciravegna, Fabrizio Silvestri, Mateja Jamnik, and Pietro Lio. Encoding concepts in graph neural networks. *arXiv preprint arXiv:2207.13586*, 2022.
- [31] Junchi Yu, Tingyang Xu, Yu Rong, Yatao Bian, Junzhou Huang, and Ran He. Graph information bottleneck for subgraph recognition. In *International Conference on Learning Representations*, 2020.
- [32] Junchi Yu, Jie Cao, and Ran He. Improving subgraph recognition with variational graph information bottleneck. In *Proceedings of the IEEE/CVF Conference on Computer Vision and Pattern Recognition*, pages 19396–19405, 2022.
- [33] Siqi Miao, Yunan Luo, Mia Liu, and Pan Li. Interpretable geometric deep learning via learnable randomness injection. In *The Eleventh International Conference on Learning Representations*, 2022.
- [34] Bernhard Schölkopf, Francesco Locatello, Stefan Bauer, Nan Rosemary Ke, Nal Kalchbrenner, Anirudh Goyal, and Yoshua Bengio. Towards causal representation learning, 2021.

- [35] Yongqiang Chen, Yonggang Zhang, Yatao Bian, Han Yang, MA Kaili, Binghui Xie, Tongliang Liu, Bo Han, and James Cheng. Learning causally invariant representations for out-of-distribution generalization on graphs. *Advances in Neural Information Processing Systems*, 35: 22131–22148, 2022.
- [36] Haoyang Li, Ziwei Zhang, Xin Wang, and Wenwu Zhu. Learning invariant graph representations for out-of-distribution generalization. *Advances in Neural Information Processing Systems*, 35: 11828–11841, 2022.
- [37] David S Watson, Limor Gultchin, Ankur Taly, and Luciano Floridi. Local explanations via necessity and sufficiency: Unifying theory and practice. In *Uncertainty in Artificial Intelligence*, pages 1382–1392. PMLR, 2021.
- [38] Sander Beckers. Causal explanations and xai. In *Conference on Causal Learning and Reasoning*, pages 90–109. PMLR, 2022.
- [39] Joao Marques-Silva and Alexey Ignatiev. Delivering trustworthy ai through formal xai. In *Proceedings of the AAAI Conference on Artificial Intelligence*, volume 36, pages 12342–12350, 2022.
- [40] Adnan Darwiche and Auguste Hirth. On the (complete) reasons behind decisions. *Journal of Logic, Language and Information*, 32(1):63–88, 2023.
- [41] Benjamin Sanchez-Lengeling, Jennifer Wei, Brian Lee, Emily Reif, Peter Wang, Wesley Qian, Kevin McCloskey, Lucy Colwell, and Alexander Wiltchko. Evaluating attribution for graph neural networks. *Advances in neural information processing systems*, 33:5898–5910, 2020.
- [42] Judea Pearl. *Causality*. Cambridge university press, 2009.
- [43] Shurui Gui, Xiner Li, Limei Wang, and Shuiwang Ji. GOOD: A graph out-of-distribution benchmark. In *Thirty-sixth Conference on Neural Information Processing Systems Datasets and Benchmarks Track*, 2022. URL [https://openreview.net/forum?id=8hHg-zs\\_p-h](https://openreview.net/forum?id=8hHg-zs_p-h).
- [44] Keyulu Xu, Weihua Hu, Jure Leskovec, and Stefanie Jegelka. How powerful are graph neural networks? *arXiv preprint arXiv:1810.00826*, 2018.
- [45] Filippo Maria Bianchi and Veronica Lachi. The expressive power of pooling in graph neural networks. *Advances in Neural Information Processing Systems*, 36, 2024.
- [46] Yoshua Bengio, Nicholas Léonard, and Aaron Courville. Estimating or propagating gradients through stochastic neurons for conditional computation. *arXiv preprint arXiv:1308.3432*, 2013.
- [47] Eric Jang, Shixiang Gu, and Ben Poole. Categorical reparameterization with gumbel-softmax. *arXiv preprint arXiv:1611.01144*, 2016.
- [48] Mathias Niepert, Pasquale Minervini, and Luca Franceschi. Implicit MLE: backpropagating through discrete exponential family distributions. In *NeurIPS*, Proceedings of Machine Learning Research. PMLR, 2021.
- [49] Pablo Barceló, Egor V Kostylev, Mikael Monet, Jorge Pérez, Juan Reutter, and Juan-Pablo Silva. The logical expressiveness of graph neural networks. In *8th International Conference on Learning Representations (ICLR 2020)*, 2020.
- [50] Weihua Hu, Matthias Fey, Marinka Zitnik, Yuxiao Dong, Hongyu Ren, Bowen Liu, Michele Catasta, and Jure Leskovec. Open graph benchmark: Datasets for machine learning on graphs. *Advances in neural information processing systems*, 33:22118–22133, 2020.
- [51] Mert Kosan, Arlei Silva, and Ambuj Singh. Robust ante-hoc graph explainer using bilevel optimization, 2023.
- [52] Pang Wei Koh, Thao Nguyen, Yew Siang Tang, Stephen Mussmann, Emma Pierson, Been Kim, and Percy Liang. Concept bottleneck models. In *International Conference on Machine Learning (ICML)*, volume 119 of *Proceedings of Machine Learning Research*, pages 5338–5348. PMLR, 2020.

- [53] Emanuele Marconato, Andrea Passerini, and Stefano Teso. Glancenets: Interpretable, leak-proof concept-based models. In *NeurIPS*, 2022.
- [54] Chirag Agarwal, Sree Harsha Tanneru, and Himabindu Lakkaraju. Faithfulness vs. plausibility: On the (un)reliability of explanations from large language models, 2024.
- [55] Wojciech Samek, Grégoire Montavon, Sebastian Lapuschkin, Christopher J. Anders, and Klaus-Robert Müller. Explaining deep neural networks and beyond: A review of methods and applications. *Proceedings of the IEEE*, 109(3):247–278, 2021. doi: 10.1109/JPROC.2021.3060483.
- [56] Raphael Suter, Djordje Miladinovic, Bernhard Schölkopf, and Stefan Bauer. Robustly disentangled causal mechanisms: Validating deep representations for interventional robustness. In *International Conference on Machine Learning*, pages 6056–6065. PMLR, 2019.
- [57] Bernhard Schölkopf, Francesco Locatello, Stefan Bauer, Nan Rosemary Ke, Nal Kalchbrenner, Anirudh Goyal, and Yoshua Bengio. Toward causal representation learning. *Proceedings of the IEEE*, 2021.
- [58] Steve Azzolin, Antonio Longa, Pietro Barbiero, Pietro Lio, and Andrea Passerini. Global explainability of gnns via logic combination of learned concepts. In *The Eleventh International Conference on Learning Representations*, 2022.
- [59] Sergey N Dorogovtsev and Jose FF Mendes. Evolution of networks. *Advances in physics*, 51(4):1079–1187, 2002.
- [60] Zhenqin Wu, Bharath Ramsundar, Evan N Feinberg, Joseph Gomes, Caleb Geniesse, Aneesh S Pappu, Karl Leswing, and Vijay Pande. Moleculenet: a benchmark for molecular machine learning. *Chemical science*, 9(2):513–530, 2018.
- [61] Ines Filipa Martins, Ana L Teixeira, Luis Pinheiro, and Andre O Falcao. A bayesian approach to in silico blood-brain barrier penetration modeling. *Journal of chemical information and modeling*, 52(6):1686–1697, 2012.
- [62] Federico Monti, Davide Boscaiini, Jonathan Masci, Emanuele Rodola, Jan Svoboda, and Michael M Bronstein. Geometric deep learning on graphs and manifolds using mixture model cnns. In *Proceedings of the IEEE conference on computer vision and pattern recognition*, pages 5115–5124, 2017.
- [63] Eric Jang, Shixiang Gu, and Ben Poole. Categorical reparameterization with gumbel-softmax. In *International Conference on Learning Representations*, 2017. URL <https://openreview.net/forum?id=rkE3y85ee>.
- [64] Ashish Vaswani, Noam Shazeer, Niki Parmar, Jakob Uszkoreit, Llion Jones, Aidan N Gomez, Łukasz Kaiser, and Illia Polosukhin. Attention is all you need. *Advances in neural information processing systems*, 30, 2017.



## A Proofs

### A.1 Proof of Proposition 1

**Proposition 1.** (Informal.) Let  $(p_R, p_C)$  and  $(p'_R, p'_C)$  two pairs of interventional distributions. Then, depending on  $p_\theta$  and  $G_A$ ,  $|\text{Suf}_{d, p_R}(R_A) - \text{Suf}_{d, p'_R}(R_A)|$  and  $|\text{Nec}_{d, p_C}(R_A) - \text{Nec}_{d, p'_C}(R_A)|$  can be as large as the natural range of  $d$ .

*Proof.* We prove the statement for graph classification; the case of node classification is analogous.

Assume  $R_A$  attains a perfect degree of sufficiency according to  $p_R$ , i.e.,  $\text{Suf}_{p_R}(R_A) = 0$ , and take  $p'_R$  such that  $\mathcal{S} \cap \mathcal{S}' = \emptyset$ , where we shortened  $\mathcal{S} = \text{supp}(p_R)$  and  $\mathcal{S}' = \text{supp}(p'_R)$ . Also, assume that both supports are finite. Then:

$$|\text{Suf}_{p_R}(R_A) - \text{Suf}_{p'_R}(R_A)| = \left| \sum_{G'_A \in \mathcal{S}} \Delta(G_A, G'_A) p_R(G'_A) + \sum_{G'_A \in \mathcal{S}'} \Delta(G_A, G'_A) p'_R(G'_A) \right| \quad (4)$$

The two sums have no terms in common, so we can independently control the second one through our choice of interventional distribution  $p'_R$ . In fact, it is maximized by those distributions that associate all probability mass to graphs  $G'_A$  for which  $\Delta(G_A, G'_A)$  is largest, e.g., counterfactuals. As long as at least one counterfactual  $G'_A$  exists that includes  $R_A$  as a subgraph, then  $p'_R$  can allocate all probability mass to it, in which case the right sum becomes as large as  $\text{argmax}_{\mathbf{p}, \mathbf{q}} d(\mathbf{p}, \mathbf{q})$ , that is, as large as the natural range of the divergence  $d$ .

A similar reasoning applies to Nec. Take  $R_A$  such that for all  $R'_A \in \text{supp}(p_C)$  it holds that  $\Delta(G_A, G'_A) > \tau$  for some desired threshold  $\tau$ . As long as there exists a graph  $G'_A \supseteq C_A$  such that  $p_\theta(\cdot | G_A) \equiv p_\theta(\cdot | G'_A)$ , then we can always choose an interventional distribution  $p_C$  that allocates all mass to it. Hence,  $\text{Nec}_{p'_C}(R_A) = 0$  and the difference in necessity will be at least  $\tau$ .  $\square$

This simple result warrants some discussion. First, we note that the assumptions it hinges on are rather weak. Its two key requirements are that: i)  $\mathcal{S}$  and  $\mathcal{S}'$  are finite: this is the case for all existing metrics, whose interventional distributions are defined over the set of *subgraphs* of the input graph, which are finitely many; ii) The GNN admits counterfactuals that subsume  $R_A$  (for sufficiency) or inputs that subsume  $C_A$  and map to the predicted label  $\hat{y}$  (for necessity), both frequent occurrences in practice.

Second, the construction behind the proof also mimics actual differences between faithfulness metrics from the literature. In fact, ignoring differences in choice of divergence, the main difference between unfaithfulness (which allocates non-zero probability only to subgraphs obtained by deleting features from the input), fidelity minus (which deletes all edges), and robust fidelity minus (which deletes a random subset of edges at random) is exactly their interventional distributions  $p_R$ , which also happen to have either disjoint or almost disjoint supports (in which case the a similar result applies almost verbatim). Our construction then amounts to saying that there are many practical situations in which one can achieve good unfaithfulness and poor fidelity minus, or vice versa.

Let us briefly discuss the relationship between metrics having the same interventional distribution but different divergences  $d$  and  $d'$ . On the bright side, it is easy to see that, as long as both  $d$  and  $d'$  are proper divergences, an explanation  $R_A$  achieving perfect sufficiency according to one will also attain perfect sufficiency according to the other, precisely because perfect sufficiency is attained when  $\Delta(G_A, G'_A) = 0$  for all  $G'_A \sim p_R$ , which can occur if and only if both divergences are zero (by definition of divergence). The same holds for the degree of necessity. For non-optimal sufficiency and necessity, the difference due to replacing divergences is governed by well-known inequalities, such as Hölder's (between  $L_p$  distances) and Pinsker's (relating the KL to the  $L_1$  distance).

The situation is different if  $d$  is a proper divergence (say, the KL divergence) and  $d'$  is a difference in likelihoods. In this case, there are situations in which the two quantities can differ. To see this, consider a multi-class classification problem, target decision  $(G_A, \hat{y})$  and a modified input  $G'_A \sim p_R$  such that i)  $p_\theta(\hat{y} | G_A) = p_\theta(\hat{y} | G'_A)$ , but ii) the two label distributions have disjoint support. In this case, the KL divergence between them would be unbounded, yet the difference in likelihood would be null. Depending on the choice of  $p_R$ , this can yield a large difference between degrees of sufficiency (and similarly for necessity).

## A.2 Proof of Proposition 2

**Proposition 2.** Fix a divergence  $d$  and a threshold  $\epsilon > 0$ . Let  $R$  contain  $r$  truly relevant edges. Then,  $\text{RFid}_+(R)$  does not depend on  $\|R\| - r$ .

*Proof.*  $\text{RFid}_+$  corrupts the explanation  $R$  by deleting edges independently at random. Formally, let  $U_j$  be a random variable determining whether edge  $e_j$  is kept, such that  $U_j \sim \text{Bernoulli}(\kappa)$ , with  $\kappa$  a user-provided hyperparameter. As in Proposition 3, let  $\mathcal{S}_R$  be the set of all subgraphs of  $G$  obtained by leaving the complement of  $R$  unmodified, and  $\mathcal{A}_R$  those subgraphs that lead to a large enough change in likelihood, that is,  $\mathcal{A}_R = \{G' \in \mathcal{S}_R : \Delta(G, G') \geq \epsilon\}$ , we can study  $\text{RFid}_+$  in terms of how likely the corrupted graphs  $G'$  it samples have missing relevant edges, i.e.,  $P(G' \in \mathcal{A}_R)$ .

$$P(G' \in \mathcal{A}_R) = 1 - P(G' \notin \mathcal{A}_R) \quad (5)$$

$$= 1 - P(U_1 = 1, \dots, U_m = 1) \quad (6)$$

$$= 1 - \prod_{j=1}^m P(U_j = 1) \quad (7)$$

$$= 1 - \kappa^m \quad (8)$$

$$(9)$$

In the second to last step, we made use of the independence of all  $U_i$ 's. which does not depend on the number of irrelevant edges  $\|R\| - r$ .  $\square$

## A.3 Proof of Proposition 3

**Proposition 3.** Fix any divergence  $d$  and a constant budget  $b \geq 1$ . Let  $\mathcal{S}_R^b$  be the set of subgraphs of  $G$  obtained by deleting  $b$  edges from  $R$  while keeping  $C$  fixed, and  $\mathcal{A}_R^b = \{G' \in \mathcal{S}_R^b : \Delta(G, G') \geq \epsilon\}$  those subgraphs that lead to a large enough change in  $\Delta$ . Also, let  $\mathcal{S}_R = \mathcal{S}_R^1 \cup \dots \cup \mathcal{S}_R^m$  and similarly for  $\mathcal{A}_R$ . Given an explanation  $R$  containing  $r$  truly relevant edges,  $\text{Nec}(R)$  computed using a uniform  $p_C$  over  $\mathcal{S}_R$  depends on the number of irrelevant edges  $\|R\| - r$ . The same holds if  $\text{Nec}(R)$  is computed using a uniform  $p_C$  over  $\mathcal{S}_R^b$ .

*Proof.* Let  $p_C$  be the uniform distribution over  $\mathcal{S}_R$ . Then, the probability of sampling a perturbed graph  $G' \sim p_C(G)$  such that  $G' \in \mathcal{A}_R$  is exactly  $|\mathcal{A}_R|/|\mathcal{S}_R|$ . Now,  $|\mathcal{A}_R|$  is exactly  $(2^r - 1) \cdot 2^{\|R\| - r}$ , while  $|\mathcal{S}_R|$  is  $2^{\|R\|} - 1$ . Hence,  $\text{Nec}$  depends on both the number of truly relevant edges  $r$  and on the size of the explanation, as expected. When choosing instead a budget  $b$  of deletions, and a uniform  $p_C(G)$  over subgraphs with  $\|G\| - b$  edges,  $P(G' \in \mathcal{A}_R^b) = |\mathcal{A}_R^b|/|\mathcal{S}_R^b|$ . Note that  $|\mathcal{S}_R^b| = \binom{\|R\|}{b}$ , while  $|\mathcal{A}_R^b| = \sum_{c=1}^b \binom{r}{c} \binom{\|R\| - r}{r - c}$ .  $\square$

## A.4 Proof of Proposition 4

**Proposition 4.** Consider a binary classification task and an  $L$ -layer injective GNN: i) For **node classification** that only uses local aggregators. Then an explanation  $R_A$  for a decision  $(G_A, \hat{y}_u)$  is strictly faithful wrt  $p_R$  iff it subsumes  $N_L(u)$ . ii) For **graph classification**. Then an explanation  $R_A$  for a decision  $(G_A, \hat{y})$  is strictly faithful wrt  $p_R$  iff it subsumes all of  $G_A$ .

*Proof.* Before proceeding, it is useful to introduce the notion of computational graph, that is, the subgraph of  $G_A$  induced by those nodes whose messages are relevant for determining the label distribution  $P(Y_u | G_A)$  or  $P(Y | G_A)$ . For node classification, it is easy to see that for GNNs with local aggregators, the only messages reaching  $u$  are those coming from nodes within  $N_L(u)$ , and for injective GNNs all such messages impact the label distribution. For graph classification, which is implicitly global, all nodes in the computational graph are the entirety of  $G_A$ .

Next, we show that if  $R_A$  does not subsume the entirety of the computational graph, then when computing strict sufficiency we can always alter those elements of the computation graph that fall in the complement  $C_A$ . By injectivity of  $p_\theta$ , any change to the features or edges of the computational graph yields a difference in label distribution, necessarily affecting both classes, and

therefore any divergence or difference in likelihood  $d$ . It follows that  $R_A$  cannot be strictly sufficient for any  $d$ , and therefore neither strictly faithful.

The converse also holds: if  $R_A$  covers the entire computational graph, then it necessarily strictly sufficient. This is because the complement  $C_A$  has no overlap with the computational graph, so altering it has no impact on the label distribution.  $\square$

### A.5 Proof of Proposition 5

**Proposition 5.** Consider a binary classification task. Let  $p_\theta$  be a modular GNN with detector  $f$  and an injective classifier  $g$  for graph or node classification. If  $f$  is stable, i.e., it always predicts the same  $R_A$  for all  $G'_A \sim p_R$ , and implements all of the following strategies:

- **Hard Scores (HS):** it outputs binary 0–1 relevance scores;
- **Content Features (CF):** the node features of  $R_A$  are taken directly from the node features of  $G_A$ ;
- **Explanation Readout (ER):** (for graph classification only)  $\text{aggr}_G$  only aggregates embeddings from  $R_A$  (as opposed to all of  $G_A$ );

then  $R_A$  is strictly faithful.

*Proof.* The proof is constructive. By assumption of stability of  $f$ ,  $R$  remains the same for every modification to  $C_A$ . By construction, models implementing the strategies listed in Proposition 5 have the classifier  $g$  using no information outside the explanation making  $R_A$  strictly sufficient. By injectivity of  $g$ ,  $R_A$  is also strictly necessary.  $\square$

### A.6 Proof of Proposition 6

**Proposition 6.** Let  $p_\theta$  be a modular DI-GNN such that the detector  $f$  outputs graphs  $R_A$  that are maximally domain-invariant, i.e., that comprise all and only those elements that are constant across the target domains. If  $R_A$  is not strictly sufficient, then the prediction is not domain invariant.

*Proof.* We proceed by contradiction. Let  $G_A$  be an input graph such that the explanation  $R_A$  for model  $p_\theta$  and decision  $(G_A, \hat{y})$  is perfectly domain-invariant yet not strictly sufficient. We assume that the model prediction does not depend on domain-induced spurious information, meaning that every modification applied to  $C_A$  will not have any impact on the model prediction (according to  $d$ ). However, the lack of strict sufficiency implies that  $\exists G'_A \in \text{supp}(p_R)$  such that  $\Delta(G_A, G'_A) > 0$ . This means that there exists a perturbation outside of  $R_A$  that altered the model prediction, which is in contradiction with assuming that it does not depend on domain-induced information.  $\square$

### A.7 Proof of Theorem 1

**Theorem:** Let  $p_\theta$  be a deterministic DI-GNN with detector  $f$  and classifier  $g$  and  $d$  be the difference in likelihood of the predicted label. Also, let  $p_\theta$  be Lipschitz with respect to changes to both the topology and the features of the input, that is, for every pair of graphs  $G_A = (G, X)$  and  $G'_A = (G', X')$ , it must hold that:

$$\left| p_\theta(Y | (G, X)) - p_\theta(Y | (G', X)) \right| \leq k_1 d_1(G, G') \quad (10)$$

$$\left| p_\theta(Y | (G, X)) - p_\theta(Y | (G, X')) \right| \leq k_2 d_2(X, X') \quad (11)$$

for suitable distance functions  $d_1$  and  $d_2$ . Then:

$$\begin{aligned} \left| \mathbb{E}_{(G_A, y) \sim p^{id}} [p_\theta(y | G_A)] - \mathbb{E}_{(G_A, y) \sim p^{ood}} [p_\theta(y | G_A)] \right| \\ \leq \mathbb{E}_{R_A^*} [k_1 (\lambda_{topo}^{id} + \lambda_{topo}^{ood}) + k_2 (\lambda_{feat}^{id} + \lambda_{feat}^{ood}) + (\lambda_{suff}^{id} + \lambda_{suff}^{ood})] \end{aligned} \quad (12)$$

Here,  $k_1, k_2 > 0$  are Lipschitz constants of  $p_\theta$ ,  $\lambda_{topo}^{id}$ ,  $\lambda_{topo}^{ood}$ ,  $\lambda_{feat}^{id}$ , and  $\lambda_{feat}^{ood}$  measure the (negated) degree of domain invariance of the detector’s output (with respect to topology and features, respectively), and  $\lambda_{suff}^{id}$ ,  $\lambda_{suff}^{ood}$  are the degree of sufficiency for ID and OOD data.

*Proof.* Let  $f^*$  be an *ideal* detector that for every input  $G_A$  outputs the maximal domain-invariant subgraph  $R_A^* = (R^*, X^{R^*})$ . Note that, for every  $(G_A^{id}, y^{id}) \sim p^{id}$  and  $(G_A^{ood}, y^{ood}) \sim p^{ood}$  that share the same invariant subgraph (that is, such that  $f^*(G_A^{id}) = f^*(G_A^{ood}) = R_A^*$ ) any DI-GNN constructed by stitching together  $f^*$  and a deterministic classifier  $g$  will predict the same label distribution for both graph, *i.e.*,  $p_g(Y | f^*(G_A^{id})) \equiv p_g(Y | f^*(G_A^{ood}))$ .

Now, fix any invariant subgraph  $R_A^*$ . When conditioning on it, it holds:

$$\mathbb{E}_{(G_A, y) \sim p^{id}(G_A, Y | R_A^*)} [p_\theta(y | f^*(G_A^{id}))] = \mathbb{E}_{(G_A, y) \sim p^{ood}(G_A, Y | R_A^*)} [p_\theta(y | f^*(G_A^{ood}))] \quad (13)$$

where the two expectations run over ID and OOD samples that share the same invariant subgraph  $R_A^*$ . We proceed by noting that:

$$\mathbb{E}_{(G_A, y) \sim p^{id}(\cdot | R_A^*)} \left| p_\theta(y | (R^*, X^{R^*})) - p_\theta(y | (R, X^{R^*})) \right| \leq k_1 \underbrace{\mathbb{E}_{(G_A, y) \sim p^{id}(\cdot | R_A^*)} [d_1(R^*, R)]}_{:= \lambda_{\text{topo}}} \quad (14)$$

The expectation on the right-hand side is the average topological distance of the predicted invariant subgraphs to  $R_A^*$ , and will be referred to as  $\lambda_{\text{topo}}$ . At the same time, it also holds that:

$$\mathbb{E}_{(G_A, y) \sim p^{id}(\cdot | R_A^*)} \left| p_\theta(y | (R, X^{R^*})) - p_\theta(y | (R, X^R)) \right| \leq k_2 \underbrace{\mathbb{E}_{(G_A, y) \sim p^{id}(\cdot | R_A^*)} [d_2(X^{R^*}, X^R)]}_{:= \lambda_{\text{feat}}} \quad (15)$$

where the expectation on the RHS is now the average distance between the features of the predicted invariant subgraphs and those of  $R_A^*$ , and will be referred to as  $\lambda_{\text{feat}}$ . Combining Eq. (14) and Eq. (15) using the triangular inequality, yields:

$$\mathbb{E}_{(G_A, y) \sim p^{id}(\cdot | R_A^*)} \left| p_\theta(y | R_A^*) - p_\theta(y | R_A) \right| \leq k_1 \lambda_{\text{topo}}^{id} + k_2 \lambda_{\text{feat}}^{id} \quad (16)$$

This holds for any fixed  $R_A^*$ .

Next, we bound the expected difference between the label distribution determined by  $R_A$  and that determined by  $G_A$  using the degree of sufficiency. For notational convenience, we draw complements  $C'_A$  rather than full modified graphs  $G'_A$  from  $p_R$ , and we denote the operation of joining  $R_A$  and  $C'_A$  to form  $G'_A$  with the  $\cup$  operator, and where we use the difference in prediction likelihood as divergence  $d$ . We proceed as follows:

$$\mathbb{E}_{(G_A, y) \sim p^{id}(\cdot | R_A^*)} \left| p_\theta(y | R_A) - p_\theta(y | G_A) \right| \quad (17)$$

$$= \mathbb{E}_{(G_A, y) \sim p^{id}(\cdot | R_A^*)} \left| \mathbb{E}_{C'_A \sim p_R(G_A)} [p_\theta(y | R_A \cup C'_A)] - p_\theta(y | G_A) \right| \quad (18)$$

$$\leq \mathbb{E}_{(G_A, y) \sim p^{id}(\cdot | R_A^*)} \mathbb{E}_{C'_A \sim p_R(G_A)} \left| p_\theta(y | R_A \cup C'_A) - p_\theta(y | G_A) \right| \quad (19)$$

$$= \mathbb{E}_{(G_A, y) \sim p^{id}(\cdot | R_A^*)} \text{Suf}(R_A) := \lambda_{\text{suff}} \quad (20)$$

$$(21)$$

In the first to second step, we made use of the law of total probability and the product rule, for which:

$$p_\theta(y | R_A) = \sum_{C'_A} p(y, C'_A | R_A) = \sum_{C'_A} \frac{p(y, C'_A, R_A)}{p(R_A)} = \sum_{C'_A} \frac{p(y | C'_A, R_A) p(C'_A | R_A) p(R_A)}{p(R_A)} \quad (22)$$

$$= \sum_{C'_A} p_\theta(y | R_A \cup C'_A) p_R(C'_A) = \mathbb{E}_{C'_A \sim p_R} p_\theta(y | R_A \cup C'_A) \quad (23)$$

Then, applying again the triangular inequality between Eq. (17) and Eq. (16) yields:

$$\mathbb{E}_{(G_A, y) \sim p^{id}(\cdot | R_A^*)} \left| p_\theta(y | R_A^*) - p_\theta(y | G_A) \right| \leq k_1 \lambda_{\text{topo}}^{id} + k_2 \lambda_{\text{feat}}^{id} + \lambda_{\text{suff}}^{id}. \quad (24)$$

The same derivation applies to  $p^{ood}(G_A)$ , so we obtain:

$$\mathbb{E}_{(G_A, y) \sim p^{ood}(\cdot | R_A^*)} \left| p_\theta(y | R_A^*) - p_\theta(y | G_A) \right| \leq k_1 \lambda_{\text{topo}}^{ood} + k_2 \lambda_{\text{feat}}^{ood} + \lambda_{\text{suff}}^{ood}, \quad (25)$$

Combining these two bounds using the triangular inequality one last time, we derive:

$$\begin{aligned} & \left| \mathbb{E}_{(G_A, y) \sim p^{id}(\cdot | R_A^*)} p_\theta(y | G_A) - \mathbb{E}_{(G_A, y) \sim p^{ood}(\cdot | R_A^*)} p_\theta(y | G_A) \right| \\ & \leq k_1 (\lambda_{\text{topo}}^{id} + \lambda_{\text{topo}}^{ood}) + k_2 (\lambda_{\text{feat}}^{id} + \lambda_{\text{feat}}^{ood}) + (\lambda_{\text{suff}}^{id} + \lambda_{\text{suff}}^{ood}). \end{aligned} \quad (26)$$

Again, this holds for all choices of  $R_A^*$ .

Finally, we leverage these inequalities to bound the difference in likelihood between ID and OOD data as follows:

$$\mathbb{E}_{R_A^*} \left[ \left| \mathbb{E}_{(G_A, y) \sim p^{id}(\cdot | R_A^*)} p_\theta(y | G_A) - \mathbb{E}_{(G_A, y) \sim p^{ood}(\cdot | R_A^*)} p_\theta(y | G_A) \right| \right] \quad (27)$$

$$\geq \left| \mathbb{E}_{R_A^*} \left[ \mathbb{E}_{(G_A, y) \sim p^{id}(\cdot | R_A^*)} p_\theta(y | G_A) - \mathbb{E}_{(G_A, y) \sim p^{ood}(\cdot | R_A^*)} p_\theta(y | G_A) \right] \right| \quad (28)$$

$$= \left| \mathbb{E}_{(G_A, y) \sim p^{id}} p_\theta(y | G_A) - \mathbb{E}_{(G_A, y) \sim p^{ood}} p_\theta(y | G_A) \right| \quad (29)$$

where  $\mathbb{E}_{R_A^*}$  runs over all possible maximally invariant subgraphs and no longer depends on the specific choice of  $R_A^*$ . By monotonicity of the expectation we conclude that:

$$\left| \mathbb{E}_{(G_A, y) \sim p^{id}} p_\theta(y | G_A) - \mathbb{E}_{(G_A, y) \sim p^{ood}} p_\theta(y | G_A) \right| \quad (30)$$

$$\leq \mathbb{E}_{R_A^*} \left[ k_1 (\lambda_{\text{topo}}^{id} + \lambda_{\text{topo}}^{ood}) + k_2 (\lambda_{\text{feat}}^{id} + \lambda_{\text{feat}}^{ood}) + (\lambda_{\text{suff}}^{id} + \lambda_{\text{suff}}^{ood}) \right] \quad (31)$$

□

## B Experimental Details

### B.1 Datasets

In this study, we conduct an investigation across seven graph classification datasets commonly used for evaluating SE-GNNs and DI-GNNs. Specifically, we examine three synthetic datasets and four real-world datasets, and in the following paragraphs, we provide a detailed description of each.

#### Synthetic datasets

- **BaMS** [58] is a synthetic dataset consisting of 1,000 Barabasi-Albert (BA) graphs, each with network motifs (house, grid, wheel) randomly attached at various positions. Class 0 includes plain BA graphs and BA graphs enriched with either a house, a grid, a wheel, or all three motifs together. Class 1 consists of BA graphs enriched with a combination of two motifs: a house and a grid, a house and a wheel, or a wheel and a grid. This dataset is utilized in the context of self-explainable Graph Neural Networks (GNNs), with the expected ground truth explanations being the specific motif combinations in each class.
- **Motif2-Basis** [18] is a synthetic dataset comprising 24,000 graphs categorized into three classes. Each graph consists of a basis and a motif. The basis can be a ladder, a tree (or a path), or a wheel. The motifs are a house (class 0), a five-node cycle (class 1), or a crane (class 2). The dataset is divided into training (18,000 graphs), validation (3,000 graphs), and test sets (3,000 graphs). In the context of OOD analysis, two additional sets are considered: the OOD validation set and the OOD test set. In these sets, the class-discriminative subgraph  $R_A$  (i.e., the motifs) remains fixed, while the bases are varied. Specifically, the basis for the OOD validation set (3,000 graphs) is a circular ladder, and the basis for the OOD test (3,000 graphs) set is a Dorogovtsev-Mendes graph.[59].
- **Motif-Basis** [43] is specular to **Motif2-Basis**, where the OOD test set contains graphs generated connecting the three motifs above to simple line paths of varying length.



- **Motif-Size** [43] is a synthetic dataset consisting of 24,000 graphs categorized into three classes. Similar to **Motif2-Basis**, each network is composed of a basis and a motif, with the motif serving as the class-discriminative subgraph  $R_A$ . The basis structures include a ladder, a tree (or a path), a wheel, a circular ladder, or a star. The motifs are a house (class 0), a five-node cycle (class 1), or a crane (class 2). The dataset is divided into training (18,000 graphs), validation (3,000 graphs), and test sets (3,000 graphs). In the context of OOD analysis, the size of the basis is increased. Specifically, in the OOD validation set (3,000 networks), the basis sizes are increased up to three times their original size, while in the OOD test set (3,000 networks), the basis sizes are increased up to seven times.

## Real-world datasets

- **BBBP** [60] is a dataset derived from a study on modeling and predicting barrier permeability [61]. It comprises 2,050 compounds, with 483 labeled as positive and 1,567 as negative.
- **CMNIST** [43] contains 70,000 graphs of hand-written digits transformed from the MNIST database using superpixel techniques [62]. The digits are colored according to their domains and concepts. In the training set, which contains 50,000 graphs, the digits are colored using five different colors. To evaluate the model’s performance on out-of-distribution data, the validation and testing sets each contain 10,000 graphs with two new colors introduced specifically for these sets.
- **LBAPcore** [18] is a molecular dataset consisting of 34,179 graphs sourced from the 311 largest chemical assays. The validation set comprises 19,028 graphs from the next largest 314 assays, while the test set includes 19,302 graphs from the smallest 314 assays.
- **SST2** is a sentiment analysis dataset based on the NLP task of sentiment analysis, adapted from the work of Yuan et al. [8]. In this dataset, each sentence is transformed into a grammar tree graph, where individual words serve as nodes and their associated word embeddings act as node features. The primary task is a binary classification to predict the sentiment polarity of each sentence. The dataset comprises 70,042 graphs, divided into training, validation, and test sets. The out-of-distribution (OOD) validation and test sets are specifically created to evaluate performance on data with longer sentence lengths.

## B.2 Implementation Details

**Training and reproducibility** The models are developed leveraging repositories provided by previous work. Specifically:

- **CIGA**, **LECI** and **GSAT** are developed based on the repository from [18], using commit fb39550453b4160527f0dcf11da63de43a276ad5.
- **RAGE** is implemented using the code available at <https://anonymous.4open.science/r/RAGE> as described in [51].
- For **GISST**, we use the repository from <https://anonymous.4open.science/r/SEGNNEval>, following the approach outlined in [23].

To encourage reproducibility, we stick to the hyperparameters provided in each respective repository. Model selection was performed on the ID validation set.

**Computing faithfulness** Our practical implementation of **Nec** follows the guidelines presented in Section 3.2. The idea is that choosing a fixed budget depending, for example, on a dataset-wide statistic is a simple yet sensible choice for a necessity metric properly accounting for the number of irrelevant edges present in an explanation. Specifically, we chose the budget  $b$  as a fixed proportion of the average number of undirected edges for each split of the dataset, where the proportion ratio is set to 5% in all our experiments. For each explanation, we sample a number  $q_1$  of intervened graphs, where  $q_1$  is fixed at 8 in our experiments.

For **Suf**, instead, we replace the complement of the explanation with that of a random sample from the same data split, joining with random connections the original explanation with the sampled complement. We repeat this operation for a number  $q_1$  of samples for each explanation, where  $q_1$  is fixed at 8 in our experiments, as for **Nec**.

The final faithfulness corresponds to the harmonic mean of the normalized Nec and normalized Suf scores, where we set  $d$  as the  $L_1$  divergence for both metrics, and it is computed over a subset of  $q_2$  of input graphs, which is set to 800 in our experiments. An ablation study to compare the resulting scores across a varying number of samples  $q_2$  and interventions  $q_1$  is provided in Fig. 7 and Fig. 8.

**Computing the degree of invariance** The degree of invariance appearing in Theorem 1 represents how close the predicted subgraph  $R_A$  is to the truly domain-invariant input motif, which is assumed to be the only stable factor enabling for stable predictions across domains. Carrying over the terminology from XAI, we compute this quantity as the *plausibility* [5] of the provided subgraph with respect to a known ground truth. Specifically, we compute the topology-wise degree of invariance as the Weighted Intersection over Union (WIoU) between the provided explanation relevance score, and the expected ground truth scores, which equal 1 for the invariant edges in the graph, and 0 for the others. The feature-wise degree of invariance, instead, is unmeasured as the ground truth over invariant features is typically overlooked, and no settled evaluation testbed is available.

**Implementation of faithfulness-enforcing strategies** As stated in Section 4.2, we modified the official source code of several models to implement the strategies proposed in Proposition 5.

- **Explanation Readout (ER)** The Explanation Readout strategy computes the graph embedding by applying an aggregator solely to  $R_A$ . This involves multiplying the node mask with the node embedding before performing the final global readout. Since explanations are soft scores over  $G_A$ , this approach ensures the model adheres more closely to the soft mask.
- **Hard Scores (HS)** To enforce the generation of binary 0-1 explanation masks by the detector  $f$ , we apply a technique similar to the Straight-Through (ST) trick used in the discrete Gumbel-Softmax Estimator [63]. Specifically, during the forward pass, we utilize the binary version of the mask, while in the backward pass, we use the continuous version.
- **Local aggr (LA)** To enhance the expressivity of Graph Neural Networks (GNNs), some models incorporate virtual nodes [49, 50, 20]. We remove these virtual nodes to mitigate the risk of mixing the information of the explanation with that of its complement, which can create unwanted dependencies between pairs of nodes in the graph.

**Changes with respect to the original codebase** Here we describe two minor changes we did to the original codebas.

*Stable TopK & Permutation-Invariant Metrics.* We found the original implementation of the topK operator to exhibit instabilities when used on GPU, in particular in the presence of equal scores for which alternatively the first or the last elements of the tensor are returned. This results in order-dependent metric values, either over- or under-estimated according to the order of ground truth edges in the graph<sup>7</sup>.

To avoid this bias and to have more predictable behavior, we switched to a stable implementation of the topK operator which always selects elements with the same score as they appear in the input tensor, and we randomly permute nodes and edges in each graph at loading time.

*Undirected Explanation Scores.* Accordingly to the original version of the codebase introduced in Training and Reproducibility paragraph, LECl, and GSAT are averaging the edge attention scores among directions for each undirected edge via `torch_sparse.transpose`. However, we found that, even by sticking to the original package versioning, the way `torch_sparse.transpose` is used is not weighting edge scores as expected, but rather is acting as an identity mapping. To fix this bug and to produce undirected edge scores without changing the edge attention mechanism, we average the edge scores via `torch_geometric.to_undirected`. More details are available in our codebase.

Table 5 compares performance scores for directed vs undirected explanation scores showing comparable performance aggregated over all datasets and models.

Dataset / Model	LECI	CIQA	GSAT	LECI (D)	CIQA (D)	GSAT (D)
Motif-Basis	72 ± 06	42 ± 02	57 ± 03	82 ± 05	50 ± 05	52 ± 04
Motif2-Basis	85 ± 07	46 ± 10	75 ± 06	81 ± 06	40 ± 03	77 ± 05
Motif-Size	41 ± 06	43 ± 05	51 ± 03	54 ± 06	47 ± 02	52 ± 04
SST2-Length	83 ± 01	76 ± 06	79 ± 04	83 ± 01	77 ± 04	81 ± 02
LBAPcore-Assay	71 ± 00	69 ± 01	70 ± 00	72 ± 00	70 ± 01	71 ± 00
CMNIST-Color	26 ± 10	23 ± 03	25 ± 04	28 ± 17	21 ± 03	38 ± 04

Table 5: Model performance scores for directed vs undirected explanation scores. Models labeled with '(D)' use directed edge scores.

Dataset / Model	GIN		LECI		GSAT	
	ID val.	OOD test	ID val.	OOD test	ID val.	OOD test
SST2-Length	91 ± 00	80 ± 01	92 ± 00	83 ± 01	91 ± 00	79 ± 04

Table 6: Model performance scores for SST2-Length on ID validation set and OOD test set.

## C Further Experiments

### C.1 Failure case

As discussed in Section 4.2, SST2-Length is a particularly challenging dataset for improving faithfulness. We claim this may come from the task benefiting from global information being used, which clashes with the goal of modular architectures that seek sparse and local discriminative subgraphs. Consider, in fact, the results reported in Table 6 where even a simple monolithic GNN baseline trained without any invariance-aware strategies exhibits comparable performance compared to more advanced and complex DI-GNNs. To inspect where DI-GNNs fall short, we plot in Fig. 3 the distribution of edge scores predicted by the detector of LECI and GSAT, where it is clear that they failed in identifying any sparse invariant subgraph, therefore falling back to a regular-GNN-like behavior. This is especially expected for SST2-Length, which is a graph-adapted sentiment classification dataset where node features are contextual embeddings extracted from a BERT-like Transformer [8] – which produces intrinsically globally-correlated node representations by the nature of its self-attention layers [64]. Indeed, BERT-like Transformers are the models achieving state-of-the-art performance in this task [8].

### C.2 Sensitivity of RFid+ and Nec to the explanation size

In Fig. 4, we numerically simulate the probability of deleting at least one truly relevant edge from an explanation with a growing number of irrelevant ones. The figure shows that the probability is basically insensitive to the number of irrelevant edges.

In Fig. 1 (Right) we provided an experiments showing that for GSAT, RFid+ is in fact insensible to the number of irrelevant edges in the explanation, while Nec with a suitable  $p_C$  is not. In Fig. 5 and Fig. 6 we further show that this behavior is in fact general, and occurs across different models and datasets. Specifically, for the same setting delineated in Section 3.2, we report the results also for the LECI [18] model over LBAPcore-Assay [43] molecular benchmark.

<sup>7</sup>In synthetic datasets, ground truth edges are typically the last elements as they are attached to an already generated base-graph.

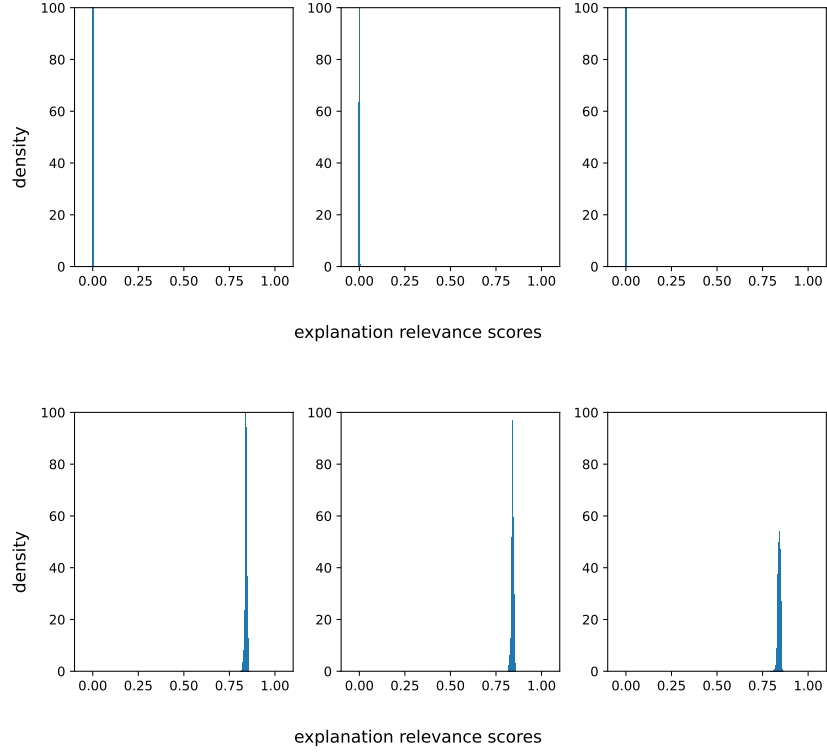


Figure 3: **Histograms of explanation relevance scores for LECI (top), and GSAT (bottom) on SST2-Length (seed 1).** Both models failed in identifying a sparse input subgraph, assigning constant scores (or very close thereof) to every edge.

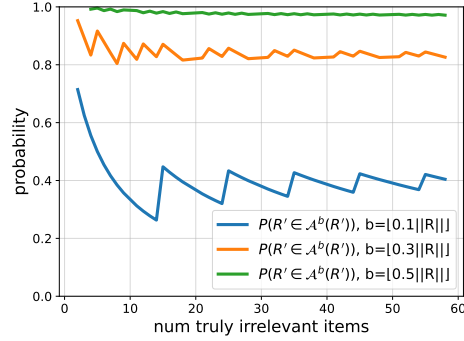


Figure 4: **Probability of deleting at least one truly relevant edge is independent of the number of irrelevant edges if the deletion budget depends on the explanation size.** Given an explanation  $R$  with  $r$  truly relevant edges ( $r = 5$ ), and a budget  $b$  proportional to the size of the explanation, the plot shows  $P(R' \in \mathcal{A}^b(R'))$  where  $R' \sim p_G^b(G)$ , for a growing number of irrelevant edges in  $R$ . The plot shows that the probability is approximately constant, i.e., it does not depend on the number of irrelevant edges. The segments with decreasing behaviour (especially visible for a 10% budget, the blue curve) correspond to areas where the budget is indeed constant, and thus not proportional to the explanation size. For instance, between 1 and 14 irrelevant edges, a budget of 10% corresponds to deleting one edge.

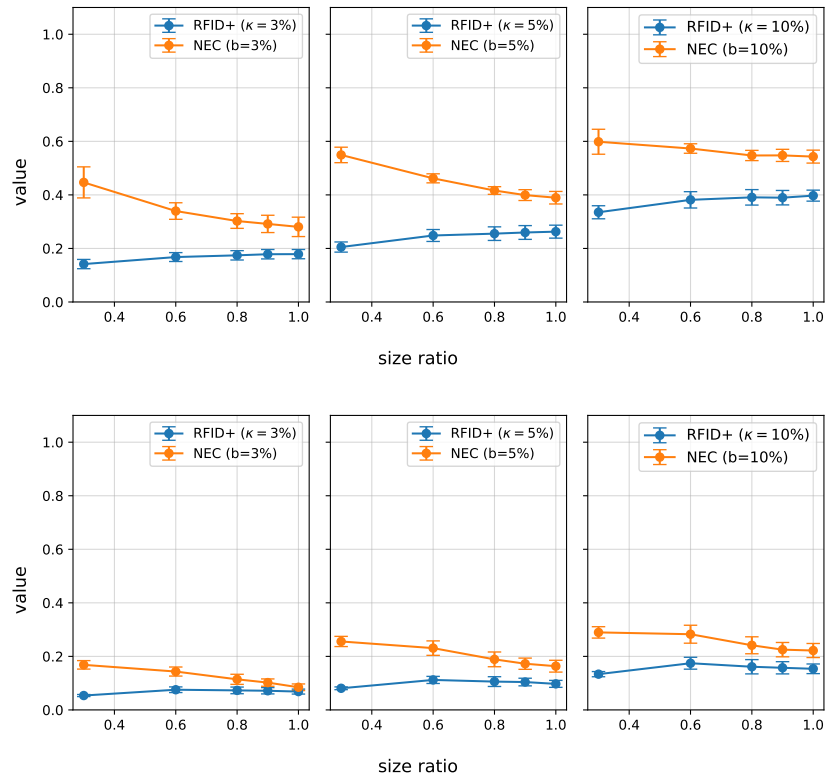


Figure 5: RFid+ is insensitive to irrelevant edges. RFid+ and Nec with  $p_C^b$  are computed for LECI and averaged across 5 seeds on Motif2-Basis (top) and LBAPcore-Assay (bottom) for different explanation sizes (x-axis) and for different metric hyper-parameter  $\kappa, b \in \{3\%, 5\%, 10\%\}$ . RFid+ assigns similar or even higher scores to larger explanations, while Nec tends to penalize larger explanations.



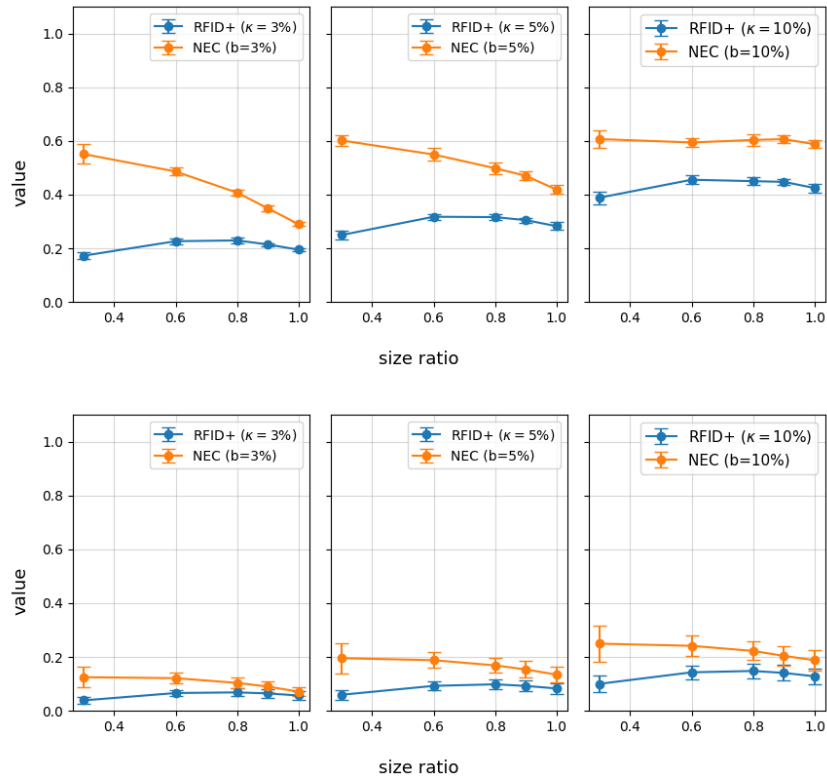


Figure 6: RFid+ is insensitive to irrelevant edges. RFid+ and Nec with  $p_C^b$  are computed for GSAT and averaged across 5 seeds on Motif2-Basis (top) and LBAPcore-Assay (bottom) for different explanation sizes (x-axis) and for different metric hyper-parameter  $\kappa, b \in \{3\%, 5\%, 10\%\}$ . RFid+ assigns similar or even higher scores to larger explanations, while Nec tends to penalize larger explanations.

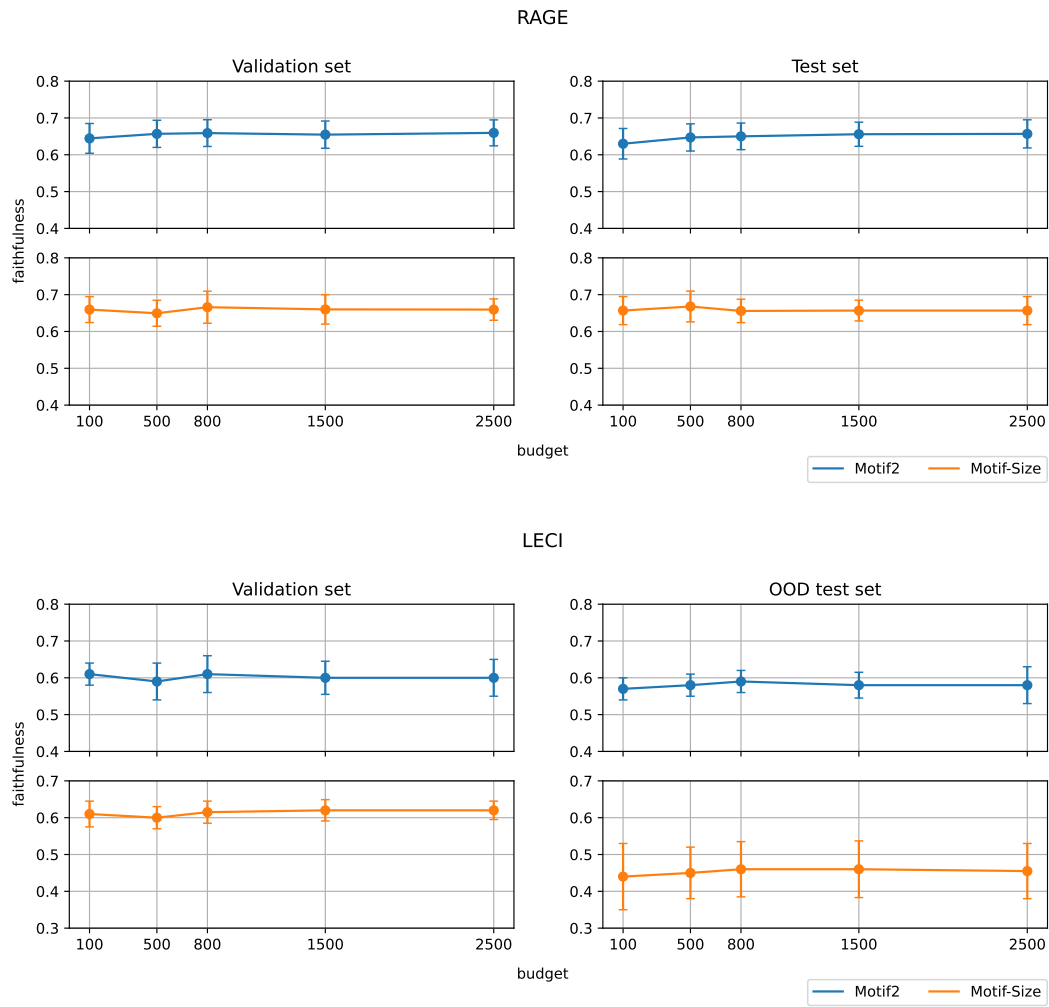


Figure 7: Ablation study of faithfulness scores across varying number of number of samples  $q_2$ .

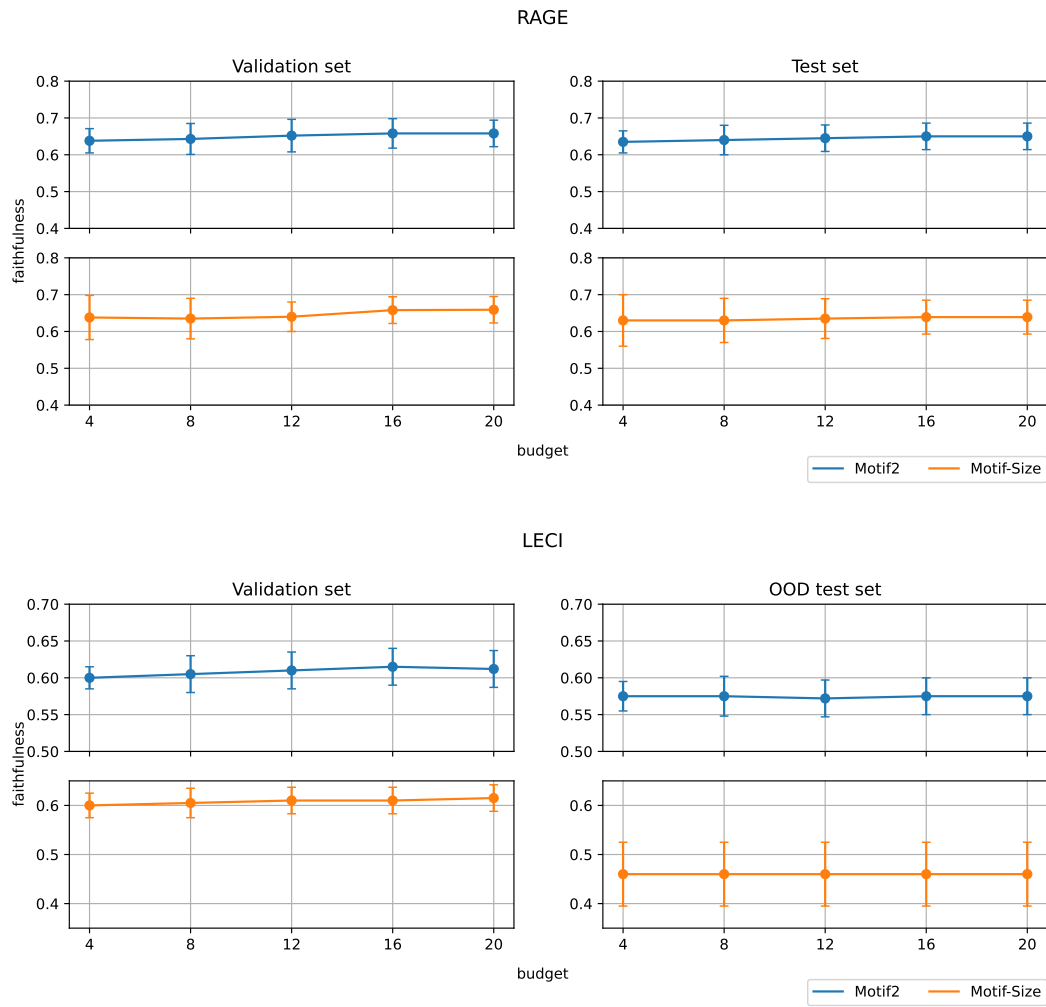


Figure 8: Ablation study of faithfulness scores across varying number of interventions  $q_1$ .